How to cite: *Angew. Chem. Int. Ed.* **2024**, *63*, e202303146
doi.org/10.1002/anie.202303146

Single Molecule Magnets

Increasing the Magnetic Blocking Temperature of Single-Molecule Magnets

Veacheslav Vieru, Silvia Gómez-Coca, Eliseo Ruiz, and Liviu F. Chibotaru**

Angewandte International Edition Chemie

Abstract: The synthesis of single-molecule magnets (SMMs), magnetic complexes capable of retaining magnetization blocking for a long time at elevated temperatures, has been a major concern for magnetochemists over the last three decades. In this review, we describe basic SMMs and the different approaches that allow high magnetization-blocking temperatures to be reached. We focus on the basic factors affecting magnetization blocking, magnetic axiality and the height of the blocking barrier, which can be used to group different families of complexes in terms of their SMM efficiency. Finally, we discuss several practical routes for the design of mono- and polynuclear complexes that could be applied in memory devices.

1. Introduction

Magnetic materials have been fascinating objects throughout the history of mankind. Magnets have been normally associated with metals and alloys, which are heavy materials with a macroscopic size. For this reason, the breakthrough in 1993 of a single molecule behaving like a magnet at the nanoscopic level[1,2] attracted great interest from both experimentalists and theorists for its potential application in technology, especially in the fields of information storage,[3–5] qubits[6–10] and spintronic devices.[4,9] Over the last three decades, a large number of single-molecule magnets (SMMs) have been synthesized and characterized, both structurally and magnetically.[11–14] Since the discovery of magnetization blocking in the polynuclear Mn_{12} $\{Mn^{III}_8Mn^{IV}_4\}$ complex (**1**, $[Mn_{12}O_{12}(O_2CMe)_{16}(H_2O)_4]$, see Figure 1a) presenting a total spin of $S=10$,[1,2] many research groups have made an enormous effort to obtain systems with improved SMM properties.[11–16] Studies have mainly focused on increasing the magnetic blocking barrier. The record of 46 cm^{-1} was held by **1** for a long period until 2007, when a higher blocking barrier of 60 cm^{-1} was reported for $S=12$ Mn_6 (**2**, $[Mn_6O_2(Et\text{-}sao)_6(O_2CPh(Me)_2)_2(EtOH)_4(H_2O)_2]$ where Et-saoH$_2$ is 2-hydroxyphenylpropanone oxime, Figure 1b).[17]

In the early years, efforts concentrated on the synthesis of polynuclear systems, mainly using Mn^{III} cations with a Jahn–Teller distortion as the source of magnetic anisotropy. A higher total spin was engineered simultaneously alongside a high axial magnetic anisotropy via ferro- or ferrimagnetic intramolecular couplings, since the energy of the blocking barrier directly depends on these two factors. However, despite the synthesis of very large clusters, no significant improvements in SMM properties were obtained. For instance, the Mn_{19} $\{Mn^{II}_7Mn^{III}_{12}\}$ system[18] (**3**, $[Mn_{19}O_8(N_3)_8(HL)_{12}(MeCN)_6]Cl_2$ where H_3L is 2,6-bis(hydroxymethyl)-4-methylphenol) has a very large spin value of $S=83/2$, but is not an SMM, whereas the Mn_{84} complex (**4**, $[Mn_{84}O_{72}(O_2CMe)_{78}(OMe)_{24}(MeOH)_{12}(H_2O)_{42}(OH)_6]\cdot x H_2O\cdot y CHCl_3$, Figure 1c), a giant wheel measuring 4.2 nm, has a ground state of $S=6$ and a blocking barrier of only 12.5 cm^{-1}.[19] The main problem of these very large systems is a failure to achieve a parallel alignment of the Jahn–Teller axes of the cations, mainly Mn^{III}. Even when this is practically achieved, as in the case of the mentioned Mn_6 complex, the magnetic anisotropy of the Mn^{III} centers is often relatively small.[20] In 2003, SMM behavior in a system with only one magnetic center was observed for the first time in a double-decker Tb^{III} phthalocyanine complex[21] (**5**, TBA[$TbPc_2$] where TBA is tetrabutylammonium and H_2Pc is phthalocyanine, Figure 1d), with a blocking barrier of around 230 cm^{-1} (larger barriers of 500–700 cm^{-1} were found later for this family of systems[22]). However, it was not until some years later that this system sparked considerable interest, with research groups focusing on mononuclear complexes containing metals that presented the highest possible magnetic anisotropy (not only lanthanides, but also transition metals), such as the first mononuclear transition metal (TM) SMM reported in 2010[23] (**6**, K[Fe(tpa^{Mes})] where tpa^{Mes} is tris(mesitylpyrrolyl-α-methyl)amine, Figure 1e). Although, for many years, the barrier for magnetization reversal was considered the Figure of merit for SMMs, the fundamental parameter for the application of SMMs is the blocking temperature. Below this temperature, the molecule behaves like a magnet. Above this temperature, the system cannot maintain the spin in its preferred orientation over a reference period of time. The blocking temperature has undergone a strong increase from that observed for the first SMMs (i.e., 3 K for **1** or 4.5 K for the widely studied **2**) to that observed for the systems with the highest known blocking temperatures (i.e., 60–80 K for derivatives of the dysprosocenium molecule (**7**, $[(Cp^{iPr5})Dy(Cp^*)][B(C_6F_5)_4]$ where Cp^{iPr5} is penta-isopropylcyclopentadienyl and Cp* is pentamethylcyclopentadienyl, Figure 1f),[24–26] reaching the liquid nitrogen limit), with energy barriers of around 1200–1500 cm^{-1}. Although the search for systems with high blocking temper-

[*] V. Vieru
Maastricht Science Programme, Faculty of Science and Engineering, Maastricht University
6229 EN Maastricht (The Netherlands)
S. Gómez-Coca, E. Ruiz
Departament de Química Inorgànica i Orgànica, Universitat de Barcelona
08028 Barcelona (Spain)
and
Institut de Recerca de Química Teòrica i Computacional, Universitat de Barcelona
08028 Barcelona (Spain)
E-mail: eliseo.ruiz@antares.qi.ub.edu
L. F. Chibotaru
Theory of Nanomaterials Group, Katholieke Universiteit Leuven
3001 Leuven (Belgium)
E-mail: liviu.chibotaru@kuleuven.be

atures has focused on mononuclear complexes in recent years, surprising results have also been found in dinuclear systems containing a coupling between the two metal centers through radicals or free electrons. As an example, the mixed-valence dinuclear lanthanide complex formed with $(Cp^{iPr5})_2Ln_2I_3$ and both Dy and Tb (**8** and **9**, $(Cp^{iPr5})_2Dy_2I_3$ and $(Cp^{iPr5})_2Tb_2I_3$ respectively, Figure 1g) results in huge coercive fields of 14 T at temperatures of 50 and 60 K, respectively.[27] This review will focus on the progress in understanding the mechanisms underlying magnetization blocking in SMMs that have produced considerable improvements in their properties, especially in the blocking temperature.

2. Slow Magnetic Relaxation in Metal Complexes

To understand the factors influencing magnetization blocking in SMMs, especially their blocking temperature, it is necessary to know the mechanisms that cause magnetization relaxation. To behave as magnets at the level of one molecule, the systems must exhibit magnetic anisotropy, i.e., a tendency to keep their spin aligned to a preferential orientation through spin-orbit coupling. Experimentally, this is seen when the spin is first aligned by an external magnetic field that is applied in the preferential direction, with the spin retaining its orientation for a period of time after the removal of the magnetic field (Figure 2a). In systems with sufficiently strong magnetic anisotropy, this behavior is also reflected in the opening of magnetic hysteresis (Figure 2b). Traditionally, the dependence of the imaginary AC magnetic susceptibility on the frequency has been also used as the fingerprint of slow spin relaxation. Indeed, when the spin has a strong tendency to be aligned in one direction, it encounters resistance in following the oscillating magnetic field. Consequently, magnetic susceptibility strongly depends on the oscillation frequency (Figure 2c).[11]

The spin relaxation time τ depends mainly on the temperature T and the presence of an external magnetic field H. In the case of a low T, when only the ground magnetic state is populated, the reversal of magnetization corresponds to the transition between its two components. τ can be calculated by Equation (1) (the entering parameters are constants that are experimentally determined from the AC magnetic susceptibility measurements). From a practical point of view, the efficiency of all these spin relaxation mechanisms should be decreased to obtain a better SMM. The first four terms in Equation (1) are temperature-dependent since they involve the participation of phonons and, therefore, depend on their population number (Figure 2d).

Liviu Chibotaru has received his Ph.D. from the Academy of Sciences of Moldova (ASM) in 1985. After working as Scientific Researcher and Senior Scientific Researcher at the Laboratory of Quantum Chemistry at ASM (1985–1995), he joined the Division of Quantum and Physical Chemistry at Catholic University of Leuven as Postdoctoral Researcher and then Associate Professor and Head of the Group of Theory of Nanomaterials. His current research focuses on the development and application of ab initio methods for the description of anisotropic magnetism in metal complexes, magnetic relaxation and magnetization blocking in single-molecule magnets.

Silvia Gómez-Coca has received her Ph.D. from Universitat de Barcelona (UB) in 2013 under the supervision of Prof. Eliseo Ruiz. She undertook postdoctoral positions at Texas A&M University (2015–2016), King's College London (2016–2018) and UB (2013–2015 and 2019–2021). Since 2021 she is a Lecturer at Universitat de Barcelona. Her current research interests are mainly in the fields of molecular magnetism, molecular electronics and supramolecular chemistry. In magnetism she focuses on the combined experimental and computational study of magnetic anisotropy and spin relaxation processes in single-molecule magnets.

Eliseo Ruiz has received his Ph.D. from the Universitat de Barcelona in 1993. After postdoctoral stays in Montreal (1993–1994) and Strasbourg (2000–2001), he joined Inorganic Chemistry Department at Universitat de Barcelona (2001) as Associate Professor, where he is now a Full Professor since 2011 and head of the Theoretical and Computational Chemistry Institute of the Universitat de Barcelona. His current research is mostly in the field of Molecular Magnetism focusing on single-molecule magnets and spin-crossover systems. Mainly in theoretical studies, but also experimentally on the effects of encapsulation of single-molecule magnets on their spin relaxation. Furthermore, in the investigation of single-molecule transport mainly in magnetic systems either using theoretical studies or by scanning tunneling microscope measurements.

Veaceslav Vieru has received his Ph.D. from Catholic University of Leuven in 2016 under the supervision of Prof. Liviu Chibotaru. He undertook postdoctoral research in the same research unit (Group of Theory of Nanomaterials) as FWO (Fond Wettenschappelijk Onderzoek Vlaanderen) fellow in 2016–2019. He joined University of Maastricht as Lecturer in 2019. He was promoted to Assistant Professor in 2023. His current research interests focus on the application of ab initio and DFT approaches for the investigation of blocking of magnetization in mononuclear and polynuclear single-molecule magnets.

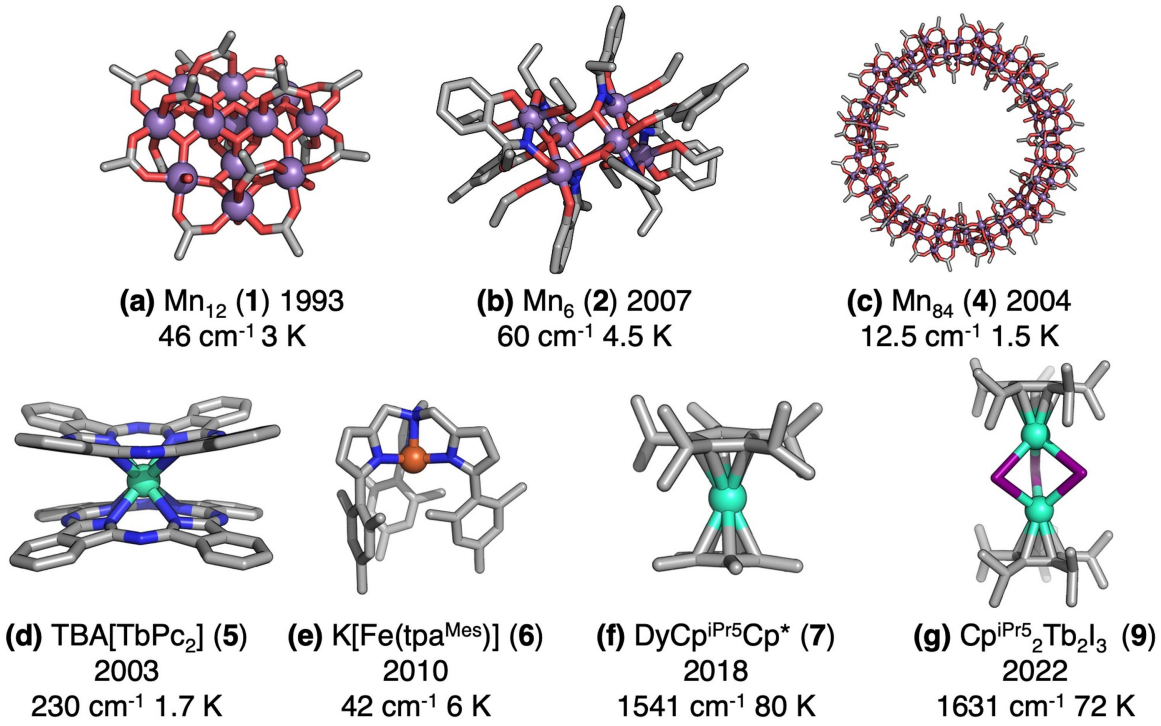

Figure 1. Structures of milestone SMMs (year, the magnetization blocking barrier and blocking temperature are indicated). (a) Mn_{12} (**1**), the first SMM; (b) Mn_6 (**2**), the first SMM with a higher barrier than that of **1**; (c) Mn_{84} (**4**), the largest polynuclear SMM; (d) TBA[$TbPc_2$] (**5**), the first Ln-based mononuclear SMM; (e) K[Fe(tpa^{Mes})] (**6**), the first transition metal-based mononuclear SMM; (f) $DyCp^{iPr5}Cp^*$ (**7**), an SMM with the highest blocking temperature; and (g) $Cp^{iPr5}{}_2Tb_2I_3$ (**9**), an SMM with a huge coercive field. All the atoms are represented as sticks, while the metals are shown as balls. The gray, red, blue and purple sticks correspond to carbon, oxygen, nitrogen and iodine atoms, respectively, while the purple, orange and light green balls represent the manganese, iron and lanthanide cations, respectively.

$$\tau^{-1} = AH^4T + CT^n + D\left(\frac{e^{-\hbar\omega/k_BT}}{\left(e^{-\hbar\omega/k_BT}-1\right)^2}\right) + \tau_0^{-1}\, e^{-\frac{U}{k_BT}} + \frac{B_1}{1+B_2H^2} \quad (1)$$

The first term, usually known as the direct process, corresponds to the one-phonon transition between the two components of the doublet in the ground state split by the external magnetic field H.[28] Its dependence on the field ($\approx H^4$) is specific to a Kramers doublet (KD) in the ground state occurring in complexes with an odd number of electrons. In non-Kramers complexes, due to an intrinsic gap in the doublet in the ground state, this term is almost field-independent at a low H, acquiring a dependence on H^2 when the Zeeman splitting of the doublet is much larger than the intrinsic gap. The linear dependence on temperature, common for both types of complexes, occurs when the intrinsic/induced gap is much smaller than the thermal energy k_BT. The second term in Equation (1) is the Raman process[29] involving a two-phonon excitation through a virtual excited state (Figure 2d) between the components of the doublet in the ground state (first-order Raman process).[28] For the sake of simplicity, it is usually considered independent of the magnetic field, which, however, seems to be unjustified for many systems. Van Vleck was the first to discover its dependence on the magnetic field by considering the effect of local vibrations (optical phonons) on the Raman relaxation process in low-spin Kramers cations.[30,31] The analysis of Raman relaxation via acoustic phonons has shown a marked dependence on the magnetic field for non-Kramers ions, with the dependence being only on the direction of H for Kramers systems.[32] The third term in Equation (1), usually called the local-mode process, is a second-order Raman process involving a localized (molecular) vibrational mode (with ω the frequency of vibration) instead of the delocalized phonon mode that is involved in the second term.[33,34] The physical interpretation of these two mechanisms offers different physical pictures.[32,35,36] The fourth term, the Orbach process, is also a two-phonon transition like the Raman mechanism, but it involves two real one-phonon processes to and from an excited state.[28] It is possible to determine the energy barrier U involved in this process and the energy of the corresponding excited state. Finally, the last term in Equation (1), the quantum tunneling of the magnetization process (QTM), is independent of temperature at a low T. It is induced by the internal hyperfine and dipolar magnetic fields originating from the nuclear spins of the surrounding atoms and magnetic moments of neighboring complexes, respectively.[37] An external magnetic field induces an energy gap between the two components of the doublet in the ground state, suppressing the tunneling relaxation. Relaxation via the tunneling of magnetization can also take place in excited

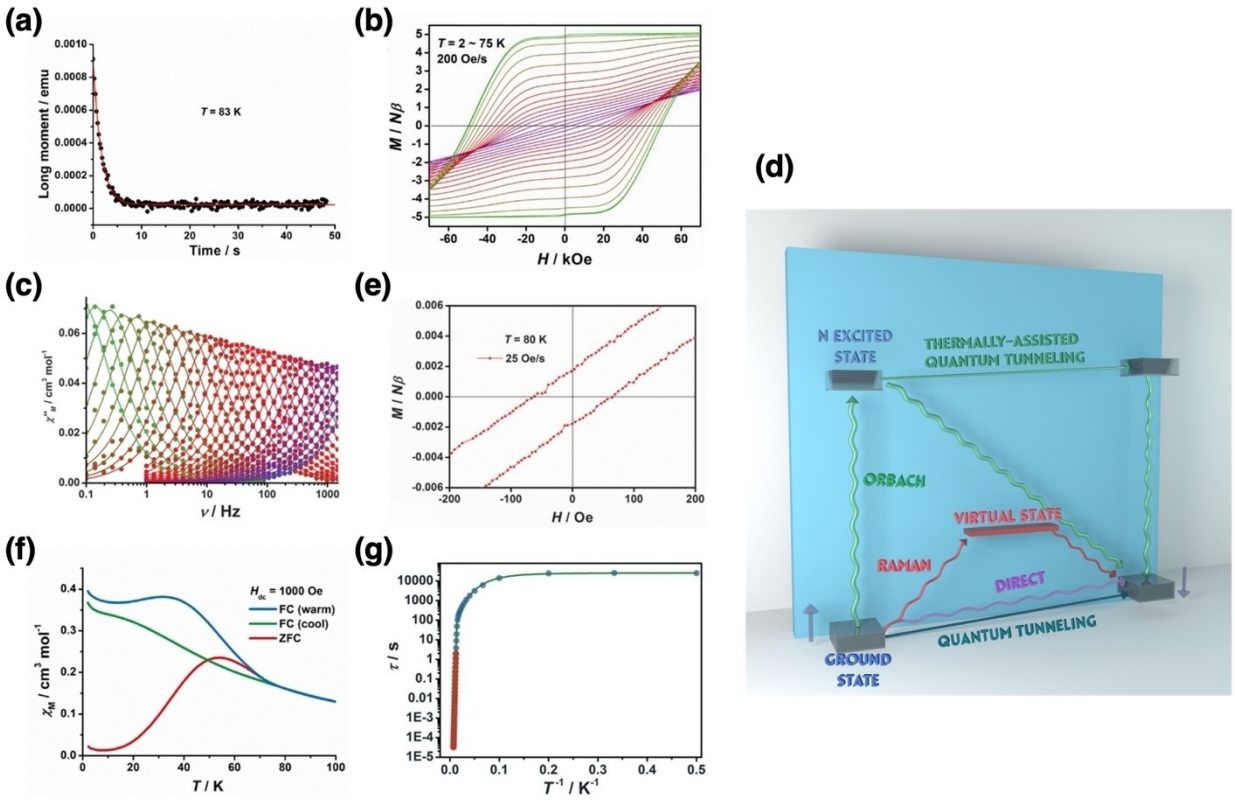

Figure 2. Magnetization blocking properties of the dysprosium metallocene cation $[(Cp^{iPr5})Dy(Cp^*)]^+$ (Cp^{iPr5}, penta-iso-propylcyclopentadienyl; Cp*, pentamethylcyclopentadienyl) (**7**), the reported system with the highest blocking temperature of 80 K:[25] (a) magnetization decay with time; (b) open hysteresis loop showing a blocking temperature above 75 K (purple curve); (c) frequency dependence of the imaginary molar magnetic susceptibility; (e) expansion of the hysteresis loops of Figure 2b at 80 K; (f) field-cooled (FC) and zero-field-cooled (ZFC) magnetic susceptibility curves; and (g) dependence of the relaxation time on temperature. Copyright 2018 American Association for the Advancement of Science. (d) Relaxation mechanisms for the dominant population of the doublet ground state. Wiggly arrows denote single-phonon transitions, while continuous arrows indicate tunneling.

states, a process called thermally-assisted quantum tunneling (TA-QTM, see Figure 2d). At sufficiently high temperatures, when this relaxation process becomes relevant, it is masked by another tunneling mechanism, the incoherent QTM based on dissipation in the phonon bath instead of nuclear spins.[11,38,39] The corresponding rate has the same dependence on H as the last term in Equation (1), as well as a dependence on temperature that is similar to the Orbach process (of course, with different parameters). Chemical strategies to suppress both tunneling processes include magnetic dilution,[40] the replacement of atoms with isotopes showing zero nuclear spin[41] or the preparation of frozen solution samples, especially using nuclear spin-free solvents.[42] It should be noted that in Kramers complexes, the internal magnetic field is the only cause of tunneling. However, in non-Kramers complexes, there is also an intrinsic tunneling gap that contributes to the QTM, which cannot be suppressed by these strategies.

Usually, the figure of merit for SMMs is the blocking temperature (T_B), with the system behaving like a magnet below it. The systems with a higher T_B are mainly limited by Orbach relaxation, while those with a lower T_B also show important contributions from other relaxation mechanisms.[43] The experimental values of T_B can be determined by three different procedures: (i) as the highest T when the hysteresis is still open for a given field sweep rate (Figure 2e); (ii) as the T-point of divergence of field-cooled and zero-field-cooled magnetic susceptibility (Figure 2f); or (iii) as the highest temperature when the spin relaxation time still exceeds a certain value, usually 100 s (Figure 2g). These different definitions can produce small differences of a few K for systems with high blocking temperatures. We would like to stress that unlike in extended magnetic materials and magnetic nanoparticles, the T_B in SMMs is a purely conventional quantity since it is defined with respect to an arbitrary reference relaxation time τ, above which the system is considered blocked. The latter, however, is strongly T-dependent in the high-temperature domain, as can be seen in Figure 2g. The same is true for remanent magnetization and the coercive field (the width of hysteresis along the H axis), which are defined with reference to a given field sweep rate and both vanish when this rate is sufficiently slow.

2.1. Assessment of spin-phonon contributions to relaxation

Spin-phonon mechanisms play a dominant role in spin relaxation when the thermal population of the relevant vibrational modes becomes sufficiently large, which is always the case when magnetization blocking is considered in complexes with a high T_B. Practically, it is not straightforward to identify the relevant vibrational modes for magnetic relaxation. An exception are acoustic phonon modes due to their guaranteed involvement in the direct relaxation process within the doublet ground state (Figure 2d) as well as the doublet excited states.[15,44–46] As for the more numerous optical phonon modes, their relevance to magnetic relaxation is identified via their relatively large value of the spin-phonon coupling constants. Given the molecular character of SMM crystals, in which optical phonon bands appear as slightly broadened molecular vibrations, the spin-phonon coupling constants merely reduce to the spin-vibrational ones, significantly simplifying their investigation.[47] Computational studies can calculate spin-vibrational coupling constants either ab initio as derivatives of the matrix elements between the spin-orbit states[24] and of the parameters of effective magnetic Hamiltonians[48] after molecular distortions, or by using the density functional theory (DFT) when the effects of spin-orbit coupling are relatively weak.[49–51]

A molecular vibration with a relatively large spin-vibrational coupling constant can also contribute directly to the relaxation rate equation via the local-mode term [the third term in Eq. (1)][52] if its broadening into a phonon band is sufficiently small.[53] Experimentally, the frequencies of the vibrational modes relevant in magnetic relaxation can be corroborated by far-infrared magnetic spectroscopy (FIRMS) measurements.[54,55] This technique assesses the strength of the spin-vibrational coupling between various pairs of magnetic levels by analyzing the changes in the spectrum induced by an applied strong magnetic field. These changes occur for phonon frequencies close to the energy separation between two magnetic levels, thus making FIRMS a complementary method that provides information on electronic state transitions such as inelastic neutron scattering[55] and high-field electron paramagnetic resonance.[54] From a synthetic point of view, to lengthen the spin relaxation process of a molecule, it is necessary to eliminate or modify the vibrational modes with high spin-vibrational coupling constants.[24,46]

The analysis of spin-vibrational coupling has been undertaken by different research groups to study the effect of the substituents in dysprosocenium complexes (see **7** in Figure 1) on the vibrations relevant for relaxation. This has revealed that substitutions in the cyclopentadiene ligands can eliminate the most efficient vibrational modes.[24–26] As a general rule, reducing the flexibility of the molecule to eliminate low-energy vibrational modes normally leads to less efficient spin relaxation. A further step in this theoretical study is the use of master equations to determine the time dependence of the spin density matrix through the solving of the Redfield equation.[32,56] There are different computational options on how to handle such an equation, but such approaches can be used to analyze spin dynamics and even estimate the coherence time T_1 of the spin-lattice relaxation.[24,57] It should be noted, however, that spin-spin relaxation (T_2 coherence time) is usually the most efficient relaxation mechanism for spin qubits, especially at low temperatures, when T_2 is shorter than T_1 and, consequently, it is the key factor for the coherence time.[9,10,46]

3. Magnetization Blocking in Mononuclear Complexes

The origin of slow spin relaxation in magnetic molecules is the strong magnetic anisotropy caused by the spin-orbit coupling on the metal ions. The latter splits the manifold of $2S+1$ degenerate states of the ground S term on the metal center into several levels, each of which (when still degenerate) is characterized by preferred directions of magnetization (magnetic anisotropy). As mentioned above, magnetization blocking occurs when the relaxation processes leading to the reversal of magnetization are suppressed. This implies the quenching of transitions between the states with opposite directions of the magnetic moment, corresponding to the left and right sides in the diagrams of magnetic levels (lower plots) in Figure 3. To do so, the low-lying spin-orbit doublets of the complex should possess high magnetic axiality.[58] This is reflected by their g tensor showing negligible transversal main values (g_x and g_y) in the case of Kramers ions or a negligible intrinsic tunneling gap in the case of non-Kramers complexes. Large magnetic axiality of a spin-orbit doublet manifests into a definite projection of the magnetic moment (M) on a common axis in its two components ($|M|$ and $-|M|$, respectively). This results in a rapid decrease in the strength of the relaxation transitions (direct, one-phonon, Raman and QTM) when the difference between the magnetic moment projections of the involved states, $\Delta M = M_2 - M_1$, becomes large.[59] As a result, in strongly axial complexes at temperatures close to the T_B, relaxation basically proceeds via several doublet excited states, with the lower ones being effectively blocked. This relaxation process involves similar mechanisms as those in the case of the dominantly populated ground state [Eq. (1)], which now scales with the Boltzmann factor corresponding to the population of this excited state, $\tau^{-1} = \tau_0^{-1} \exp(-U/kT)$. The activation energy U corresponds approximately to the energy of the doublet excited state involved in the spin relaxation and is called the blocking (or spin reversal) barrier.[11,60] For example, in Mn_{12} (**1**), the relaxation process at $T > 2$ K effectively proceeds via the sixth doublet excited state (Figure 3a), with the main contribution to τ_0^{-1} coming from TA-QTM due to the relatively small ΔM and the consequently large tunneling in this excited state.[11] On the contrary, in weakly axial complexes, the relaxation process takes place only via the ground state and the first doublet excited state (Figure 2d) in a wide temperature range. In such cases, other relaxation mechanisms besides the over-barrier one become relevant, primarily Raman relaxation.[59,61,62] However, in complexes exhibiting a high

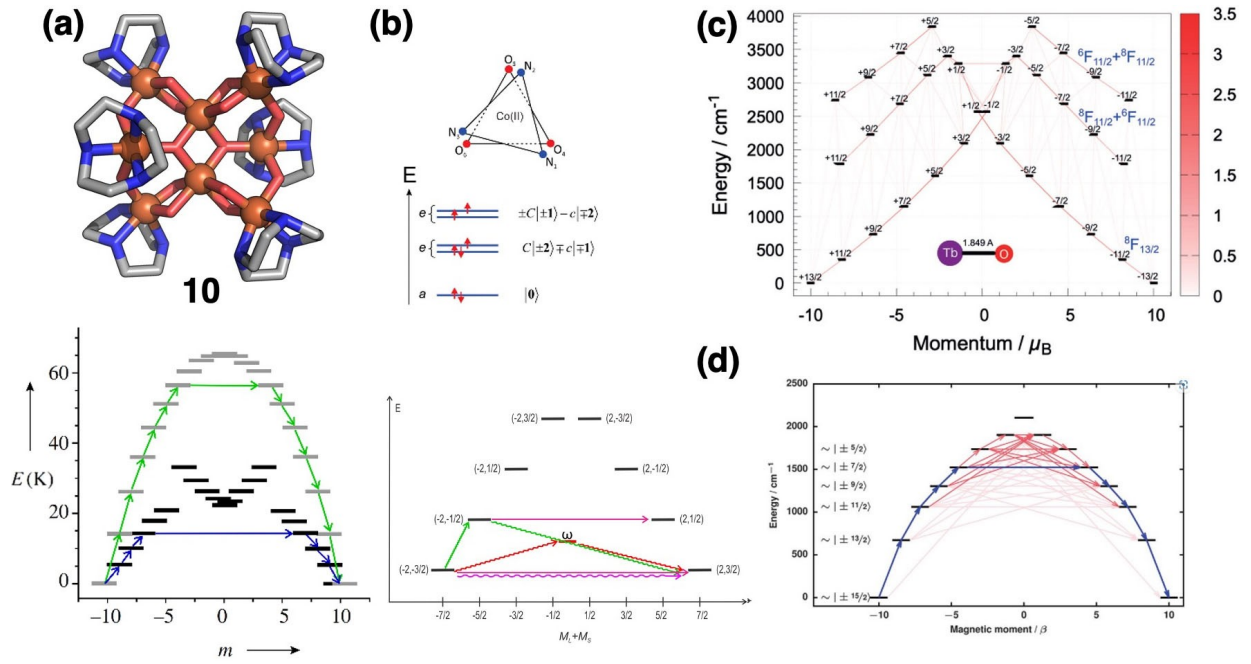

Figure 3. (a) Molecular structure of Fe_8 (**10**) and the structure of the magnetic levels $|SM>$ of the ground $S=10$ term in the Mn_{12} (**1**, gray) and Fe_8 (**10**, black) complexes.[11] The gray, red and blue sticks correspond to carbon, oxygen and nitrogen, respectively, while the orange balls represent iron cations. Copyright 2006 Oxford University Press. The green and blue arrows outline the corresponding relaxation paths. (b) A structure of orbital splitting in a trigonal prismatic configuration of a Co^{II} fragment.[64] Copyright 2013 American Chemical Society. The lower plot shows a generic scheme of the spin-orbit doublet levels in $S=3/2$ complexes with an unquenched orbital momentum (numbers in brackets are M_L, M_s values of the corresponding level). (c) *Ab initio* calculated multiplet structure of the [TbO] diatomic complex[65] (copyright 2020 Wiley-VCH), which reproduces quantitatively the infrared laser spectroscopy data.[66] (d) *Ab initio* calculated multiplet structure corresponding to the $J=15/2$ ground atomic multiplet of Dy^{III} from the complex $DyCp_2$ (**7**, Figure 1g). The intensity of the lines connecting the different levels scales with a relative value of the corresponding transition magnetic moment.[25] Copyright 2018 American Association for the Advancement of Science.

T_B, the over-barrier relaxation process, including the QTM via highly excited states lying under the top of the barrier, is the dominant mechanism underlying the reversal of magnetization, conferring an overall activation temperature dependence to the relaxation rate with a high Arrhenius activation energy.

3.1. Design principles

One factor enhancing magnetic axiality is the high rotational symmetry of the complex. In the complexes involving metal ions with weak spin-orbit coupling, an overall symmetry axis of the order $N\geq 3$ is sufficient to produce strong axiality. Thus, the S_4 axis of Mn_{12} (**1**) (Figure 1a) ensures that the zero-field split (ZFS) components of the ground $S=10$ term have definite spin projections on the main magnetic axis ($||S_4$).[11] Another favorable factor is the large spin providing an accordingly large ΔM for low-lying doublets and ensuring their relatively high magnetic axiality even in complexes without symmetry. For example, the Fe_8 (**10**, $[Fe_8O_2(OH)_{12}(tacn)_6]Br_8$ where tacn is 1.4.7-triazacyclononane, Figure 3a) SMM, showing a relatively large non-axial anisotropy due to the lack of symmetry, is still highly axial, with U corresponding to the third doublet excited state (Figure 3a).[63] Besides high rotational symmetry, the decisive condition for obtaining high values of U is the large separation of the ZFS components of the ground spin. In this respect, the spin complexes like Mn_{12} (**1**) and Fe_8 (**10**) are not efficient, as the weak spin-orbit coupling effects on the metal sites only produce barriers of several tens of wavenumbers.

The strong effects of spin-orbit coupling arise in transition metal (TM) ions with a high local symmetry (C_N, $N\geq 3$) due to the unquenching of their orbital momentum along the symmetry axis.[28] This gives rise to a strong splitting of the molecular terms into equidistant spin-orbit doublets (see the Co^{II} system in Figure 3b), which is much larger than the ZFS splitting in Mn_{12} (**1**) and Fe_8 (**10**). The separation between neighboring doublets is proportional to the spin-orbit coupling constant and the value of the unquenched orbital momentum, with the latter determined by the population of the two orbital doublets (top of Figure 3b).[64,67,68] High symmetry is only a necessary condition for an unquenched orbital momentum, with its obtention in complexes being dependent on the population Scheme of the orbitals.[69,70] For example, the high-spin Mn^{III} ions in the Mn_{12} complex display a quenched orbital momentum despite C_4 site symmetry because the two degenerate orbitals d_{xz} and d_{yz}, which could provide a first-order orbital momentum, are evenly populated with spin up (alpha) electrons. To obtain states with a definite projection of the orbital momentum (M_L), a simple crystal field

argument tells us that the order of the symmetry axis should be $N>2l$, where $l=2$ and 3 for TM and lanthanide/actinide ions, respectively. Thus, TM ions should have a five-fold symmetry which is achieved, e.g., in pentagonal bipyramids $[M(CN)_7]^{3-}$, M=Mo, Re.[71,72] However, heavy TM complexes usually have a low spin ($S=^1/_2$), which is detrimental for magnetization blocking. First-row TM complexes with an unquenched orbital momentum can have a spin $S=3/2$ [Fe^{I} and Co^{II}] and $S=2$ [Fe^{II} and Co^{III}], but their axial symmetry is usually not higher than three-fold.

For the systems presenting a Jahn–Teller (JT) distortion, the bonding nature of the involved orbitals is crucial. Thus, for example, in the complexes of Fe^{II} or Co^{II} with low coordination numbers containing degenerate low-energy orbitals,[73] the beta orbitals can give rise to electronic structures exhibiting the JT effect (e.g., Co^{II} in Figure 3b). As basically non-bonding orbitals are involved, the energy splitting caused by the JT distortion is small, generating an electronic structure that leads to a large spin-orbit coupling.[74] Moreover, if the first transitions between the occupied and empty orbitals involve d_{xz}–d_{yz} or d_{xy}–$d_{x_2-y_2}$ pairs[75] (same absolute value of M_L, the magic pentagon rule), magnetic anisotropy of the easy-axis type arises. Meanwhile, transitions between orbitals where the absolute value of M_L changes result in easy-plane behavior. For the same reason, the non-bonding character of the occupied and first empty beta orbitals of the high-spin d^6 Fe^{II} complex (**6** in Figure 1e) or of the orbital population scheme of Co^{II} cations (Figure 3b) results in strong magnetic anisotropy.

A symmetry lower than five-fold leads to an admixture of different M_L components in the orbital doublets, opening efficient relaxation channels (Figure 3b). Even small orbital mixing causes non-negligible transversal g factors, which, e.g., for the KD ground state of a $Co^{II}O_3N_3$ fragment (Figure 3b), can be as large as 0.4, thus precluding magnetization blocking despite its perfect trigonal symmetry.[64] The strongest magnetization blocking occurs in two-coordinate trigonal $S=3/2$ complexes such as [K(2.2.2-cryptand)] [Fe(C(SiMe$_3$)$_3$)$_2$]$^-$ (**11**, $U=226\,cm^{-1}$, $T_B=4.5\,K$)[68] and Co(C(SiMe$_3$)$_3$)$_2$ (**12**, $U=450\,cm^{-1}$, $T_B=4\,K$ with respect to $\tau>1\,s$)[67] due to a relatively strong axial crystal field (CF). However, the observed magnetization hysteresis shows weak coercivity. Furthermore, the extracted blocking barriers suggest that the relaxation process proceeds via the first excited doublet state (Figure 3b), following a similar scheme as that seen in weakly axial SMMs. A departure from trigonal symmetry quickly decreases the blocking properties of the complexes, most of which cease to be SMMs.[74] An exception is the two-coordinate Co^{II} imido complex with C_2 symmetry, which shows a performance comparable to that of mononuclear SMMs with a trigonal geometry (**13**, [(sIPr)CoNDmp] where sIPr is 1,3-bis(2′,6′-diisopropylphenyl)-4,5-dihydro-imidazol-2-ylidene and Dmp is 2,6-dimesitylphenyl, $U=413\,cm^{-1}$)[76] due to the covalently bound unit $[CoN]^+$ conferring strong axiality. The high-spin $3d^6$ complexes display a weaker performance than the $3d^7$ mononuclear SMMs with a comparable geometry[77] because of a higher spin $S=2$ and the resulting smaller separation between the spin-orbit doublets.

3.2. Mononuclear Ln-based SMMs

The best mononuclear TM SMMs display a similar magnetization blocking (τ of around 1 s at a T below 5 K) to that of Mn_{12} (**1**) and even Fe_8 (**10**), despite their blocking barriers being one order of magnitude higher. This is explained by their still low spin, which leads to weakly axial relaxation scenario. For the same reason, mononuclear complexes of early actinides do not perform well.[14,78] The situation is different in lanthanide ions (Ln) with both a large ground state spin S and an unquenched orbital momentum L coupling vectorially into a total angular momentum ($\mathbf{J}=\mathbf{S}+\mathbf{L}$). Lanthanides from the r.h.s. of the series have their spin and orbital momenta coupled parallel in their ground state, resulting in a large value of J. Furthermore, those with an odd number of electrons give rise to a ground state that is a Kramers doublet, i.e., Dy^{III} or Er^{III}. They also present a very strong spin-orbit coupling, overcoming the CF splitting of the 4f shell. As a result, the structure of the molecular multiplets merely represents CF-split atomic J multiplets. In most cases, mononuclear Ln complexes and fragments do not have any symmetry, but they still display a slow relaxation of magnetization, with blocking barriers reaching values of many hundreds of wavenumbers.[14,79] Some of them show relaxation via the second excited doublet state, such as the Dy^{III} fragments in Dy_4K_2 complexes.[80]

For systems involving lanthanides, an orbital description is not as simple as that for the TM complexes due to a marked multiconfigurational character of the states involved.[81] In this sense, the use of the CF theory provides a valuable alternative, especially when relating the symmetry of the molecules to the effectiveness of the spin relaxation mechanisms such as the QTM.[59] Theoretically, systems with high magnetic anisotropy, involving TMs or lanthanides, require a methodology that can describe multiconfigurational systems, including spin-orbit coupling. Normally, the calculations used are of the complete active space self-consistent field (CASSCF) type and, if dynamical correlation is included, the calculations are complemented with the CASPT2/NEVPT2 methods, which treat these effects perturbatively, a step especially relevant for TMs. The great advantage of this ab initio approach is a non-perturbative treatment of the spin-orbit coupling on the metal sites.[82]

The limit of perfect axiality of an Ln complex, i.e., conservation of its total angular momentum projection (M_J), requires rotational symmetry of the order $N\geq 7$. This, however, has never been achieved. Apart from LnO diatomic systems, the highest rotational symmetry in Ln complexes with equatorial ligands is C_5 (**16** and **7** in Figure 4), which allows for tunneling and spin-phonon relaxation between the doublet components of opposite magnetization (Figure 3d). Hence, a complex with linear coordination should be a good synthetic target to improve magnetic properties, but such a coordination mode is not easily affordable with lanthanides.[74,87] The electron density of 4f orbitals in lanthanide ions can adopt an oblate (UFO-like shape) or prolate (rugby ball shape) spheroid form, depending on the number of electrons and the populated M_J

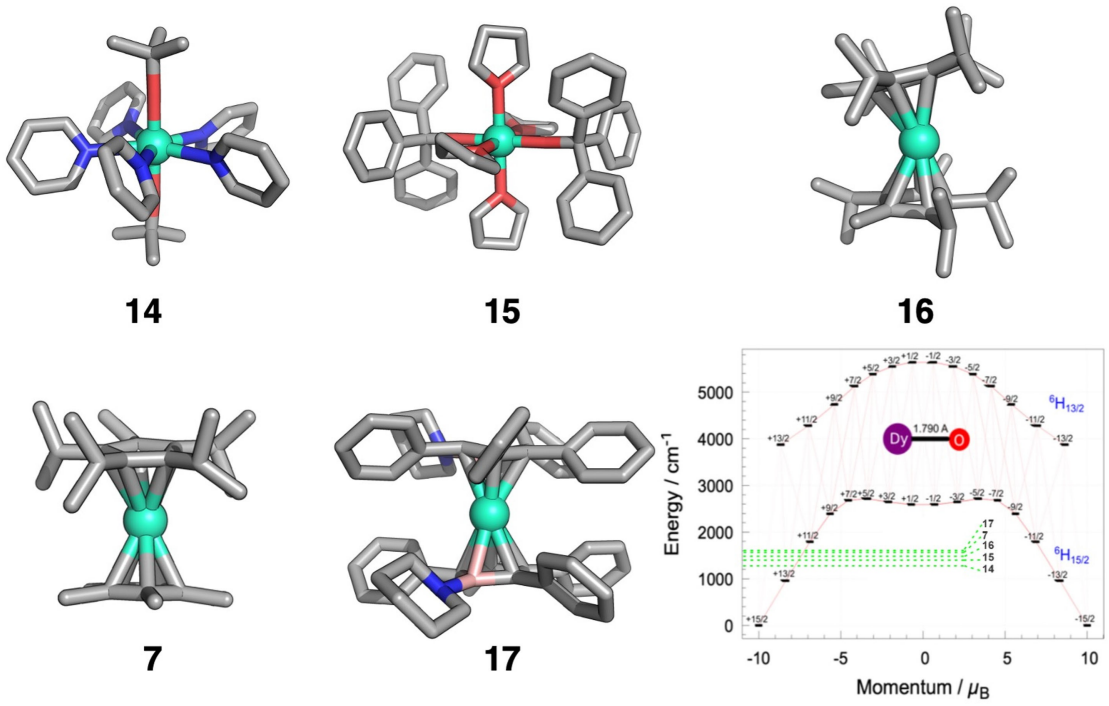

Figure 4. Mononuclear Ln-based SMMs with the highest *U*: $[Dy(O^tBu)_2(py)_5]$ (**14**),[83] $[Dy(OCPh_3)_2(THF)_4]$ (**15**),[84] $[Dy(Cp^{iPr4Me})_2]$ (**16**),[85] $[(\eta^5\text{-}Cp^*)Dy(\eta^5\text{-}Cp^{iPr5})]$ (**7**),[25] and [K(2.2.2)][[1-(piperidino)-2,3,4,5-tetraphenylborolyl]$_2$Dy] (**17**).[86] Lower right plot: *Ab initio* calculated multiplet structure of the $[DyO]^+$ diatomic system,[65] with the position of *U* for the indicated compounds shown by the green dashed lines. Copyright 2020 Wiley-VCH. All the atoms are represented as sticks, while the metals are represented as balls. Gray, red, blue and pink sticks correspond to carbon, oxygen, nitrogen and boron atoms, respectively, while the light green balls represent the dysprosium cations.

state.[88] To achieve maximum axiality, oblate ions such as Tb^{III}, Dy^{III} and Ho^{III} are desirable since the magnetization is perpendicular to the plane containing their maximal electron density.[88,59] To diminish the QTM and other spin-phonon relaxation processes in such complexes, the CF from the ligands should be as axial as possible. This means that the axial CF contributions, which conserve M_J, should provide the CF separation of the spin-orbit doublets, exceeding much the effect of the non-axial ones. In such strongly axial complexes, relaxation is pushed via a highly excited doublet state (Figure 3d), which, along with the large CF splitting of *J*, makes the blocking barrier very high. Some Ln complexes with the highest *U* are shown in Figure 4. However, a high blocking barrier does not necessarily provide an elevated T_B. Besides the presence of electron-phonon coupling between different magnetic states, efficient relaxation also requires the availability of vibrational modes matching the energy gap between these states, which varies strongly among the complexes depending on the ligands. The only mononuclear SMMs where these two factors apparently do not coexist are the dysprosocenium complexes (**7**, **16** and **17** in Figure 4).[90] Among them, the highest blocking temperature ($\tau > 100$ s), $T_B = 80$ K, has been registered for **7**.[25] While it is difficult to foresee the design of such complexes, a rule of thumb is to have a large separation between the low-lying levels, for which the number of suitable vibrations will decrease a priori.

Despite exhibiting high *U* (reaching 1600 cm^{-1} in **17**), the best mononuclear Ln-based SMMs can still only achieve half of the height of the blocking barrier for the diatomic $[DyO]^+$ system (Figure 4). This is due to important CF components originating from the ligands lying out of the main axis of symmetry. To assess their effects, we will consider a Dy^{III} complex with a perfect C_5 arrangement of five water molecules in the equatorial plane (**18**, Figure 5a),[91] whose axial CF contribution is certainly dominant. The calculated multiplet spectrum shows a relatively small splitting, with $U = 300$ cm^{-1}, which agrees with the experimental findings. For a hypothetical complex in which the water molecules have been removed from the equatorial positions, calculations show a highly axial multiplet spectrum, with $U \approx 1800$ cm^{-1} (Figure 5b).[59] Comparing these two systems, we may conclude that the axial CF components of the equatorial ligands cancel the major part of the CF originating from the axial ligands. This is a general situation that is also encountered in **15** and similar complexes.[92] Thus, the observed high blocking barrier in Ln complexes is due to the relatively weak strength of the CF components with an equatorial origin, which fails to significantly reduce the axial CF of the apical ligands.

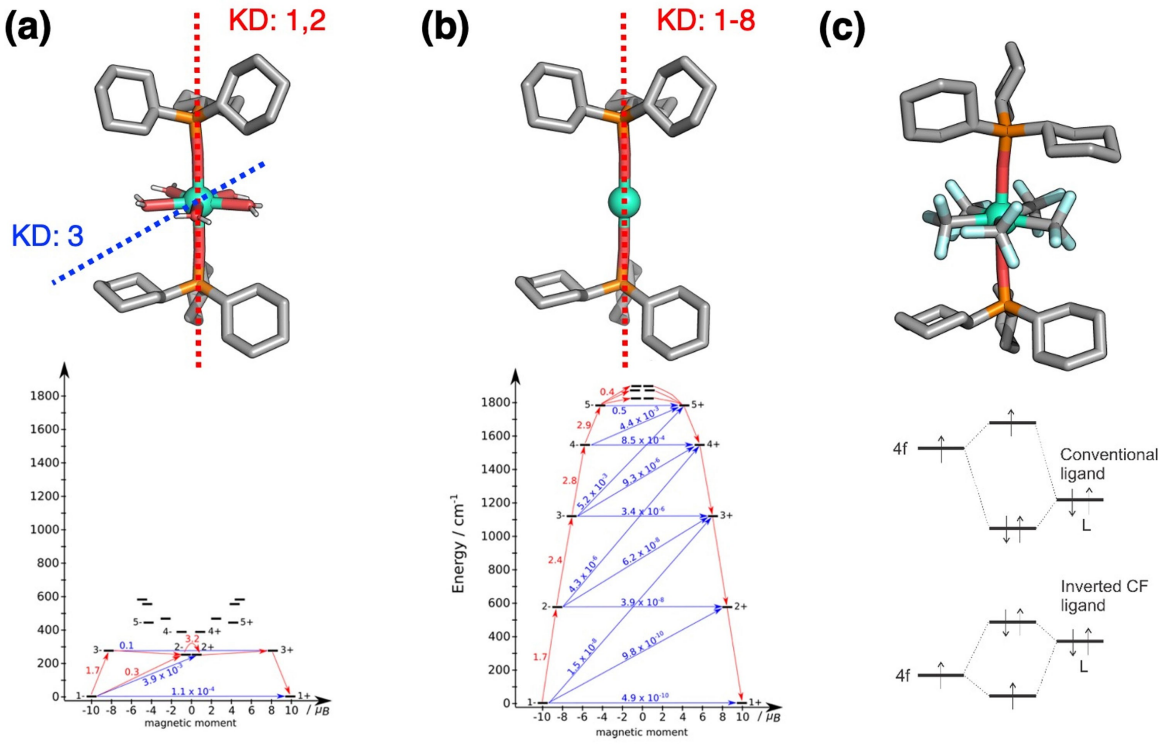

Figure 5. (a) Molecular structure and calculated low-lying multiplets of $[Dy(Cy_3PO)_2(H_2O)_5]^{3+}$ (**18**).[91] Copyright 2016 American Chemical Society. (b) The same as (a), but with the water molecules removed from the equatorial plane.[59] Copyright 2016 American Chemical Society. An underestimation of the CF splitting of the doublets by around 20% is expected due to the CASSCF approach used in the calculations. (c) Hypothetical mononuclear SMMs with five "inverted CF ligands" in the equatorial plane. All the atoms are represented as sticks, while the metals are represented as balls. Gray, red, light blue and orange sticks correspond to carbon, oxygen, fluorine and phosphorus atoms, respectively, while the light green balls correspond to the dysprosium cations.

3.3. Inverted CF ligands

The apparent drawback of equatorial ligands can be turned into an advantage if the ligands with an inverted CF[93] can be accommodated in the equatorial plane, keeping the normal ones in the apical positions (Figure 5c). These ligands will produce an axial CF of the opposite sign due to their inverted covalent effect on the metal orbitals (lower plot in Figure 5c). Such ligands have been identified in some TM complexes such as $[Cu(CF_3)_4]^{n-}$, exhibiting an inverted covalent effect for $n=1$ and 2.[94] In these complexes, the metal orbitals of the 3d type lie lower than the occupied ligand orbitals, which means that the CF splitting of the 3d orbitals resulting from the covalent interaction with the latter will give an inverted order compared to the CF splitting in similar complexes with conventional ligands (occupied ligand orbitals lying under the metal orbitals of the 3d type). Figure 6a shows the valence orbitals of $[Cu(CF_3)_4]^-$ with a planar geometry close to the D_{4h} symmetry. We can see that the four ligand orbitals of the σ type lie higher than the metallic 3d orbitals. This is naturally explained by the high oxidation state (+3) of the copper ion in this complex, resulting in low orbital energies of the Cu 3d orbitals. On the contrary, in $[Cu(CF_3)_4]^{3-}$, the oxidation state of Cu is +1 and the metallic 3d orbitals lie above the occupied ligand orbitals, thereby restoring the normal order of CF splitting. Thus, Figure 6c shows the valence orbitals for the tetrahedral geometry of $[Cu(CF_3)_4]^{3-}$ in equilibrium, where the 3d orbitals with a t_2 symmetry lie above similar orbitals with an e symmetry, which is in full agreement with the conventional CF for tetrahedral complexes. To compare with the CF splitting in $[Cu(CF_3)_4]^-$, Figure 6b shows the calculated valence orbitals for $[Cu(CF_3)_4]^{3-}$ with a similar square-planar geometry. The comparison shows a mutual inversion of the CF spectra of the 3d orbitals in these two compounds. The inversion is not perfect, however, because the CF splitting of the 3d orbitals is determined not only by the interactions with the four ligand orbitals of the σ type, but also by the interactions with the other ligand orbitals whose positions with respect to the 3d orbitals are not inverted.

This phenomenology is quite general and some ligands can be expected to manifest as "inverted CF" in Ln complexes too. Replacing the conventional ligands in the equatorial plane with inverted CF ones will further enhance the axial CF of the apical ligands instead of cancelling it.

4. Magnetization Blocking in Polynuclear SMMs

In polynuclear complexes with a weak spin-orbit coupling, such as Mn_{12} (**1**), Fe_8 (**10**) and others, the barrier arises from

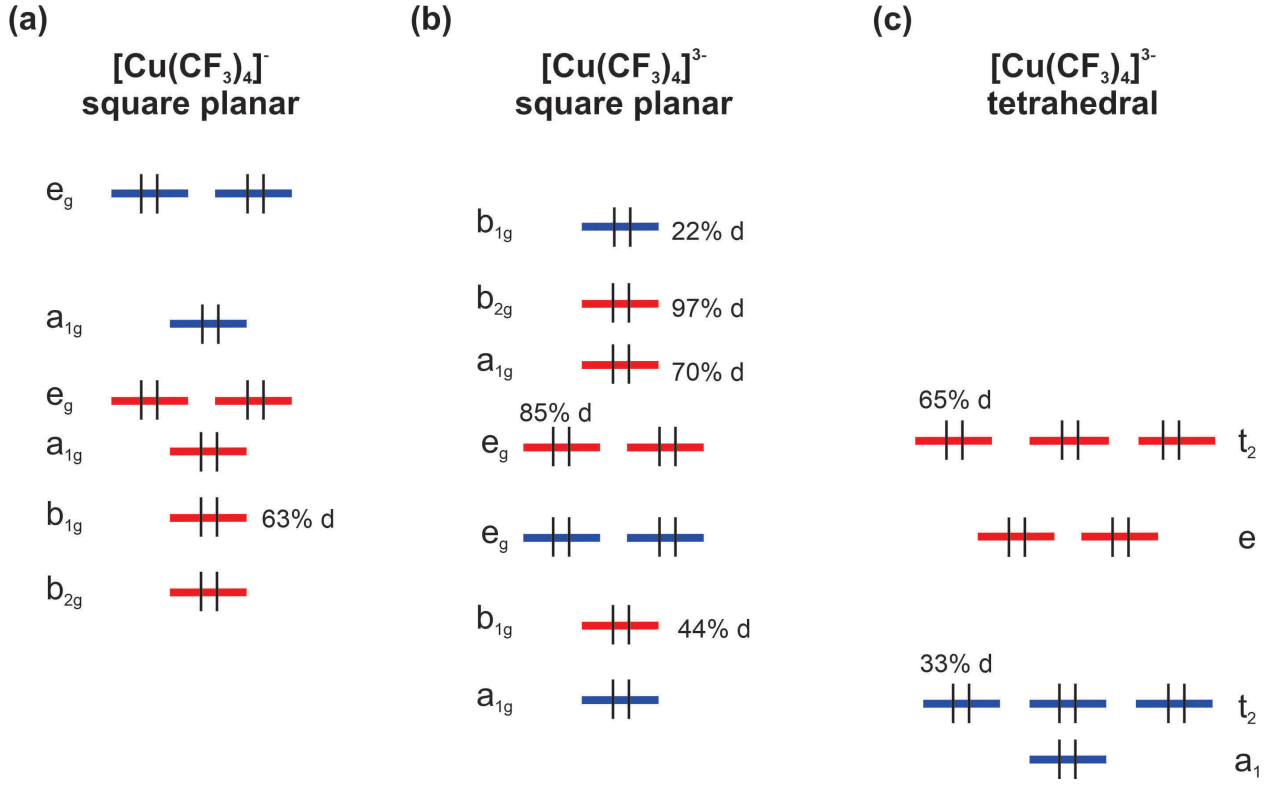

Figure 6. Valence orbitals of $[Cu(CF_3)_4]^{n-}$. Adapted with permission from Ref. [94] Copyright 2016 American Chemical Society. (a) Monoanion in equilibrium with a square-planar geometry close to D_{4h}. (b) Trianion with the same geometry as that of the previous complex. Density functional theory calculations were performed with the B3LYP functional, as described in Ref. [94]. (c) Trianion in equilibrium with a tetrahedral geometry close to T_d. The orbitals of the metal type are in red, while those of the ligand type are in blue.

the ZFS of the lowest exchange level, which is strongly separated from the first excited exchange level (SMMs of type I). As this scenario does not provide barriers higher than 100 cm^{-1}, it has been proposed that heavy TM ions (presenting large spin-orbit coupling) with axial anisotropy should be coupled to high-spin metal ions (Mn^{II} and Fe^{III}). In this scheme, the roles of magnetic anisotropy and the exchange interaction are reversed, with magnetic anisotropy producing a large separation of the spin-orbit doublets on the metal sites and the splitting of the exchange levels determining the blocking barrier,[71] which should be large due to the diffuse magnetic orbitals of the heavy metal (SMMs of type II). This strategy has been proven to be partly efficient only for $[Mn(L_{N5Me})(H_2O)]_2[Mo(CN)_7]$ (**19**, where L_{N5Me} is N,N′-bis[(1H-imidazol-4-yl)methylene]-2,2-dimethylpropane-1,3-diamine), in which the pentagonal bipyramidal $[Mo(CN)_7]^{4-}$, having a symmetry favorable to ideal axiality (see Section 3.1), is coupled to two Mn^{II} units via apical cyanides ($U = 40$ cm^{-1}, $T_B = 3.2$ K).[95] Other coordination modes of Mn^{II} ligands to the $[Mo(CN)_7]^{4-}$ core have been shown to reduce magnetization blocking, whereas coupling two complexes **19** in one unit destroys it completely.[96] The situation is pretty similar in many other mixed TM (5d–3d and 4d–3d)[97] and actinide[14,98] polynuclear complexes exhibiting weak or no SMM behavior. One of the best actinide-based SMMs is [{[Mn(TPA)I]-[UO2(Mesaldien)][Mn(TPA)I]}I] (**20**, where TPA is tris(2-pyridylmethyl)amine and Mesaldien is N,N′-(2-aminomethyl)diethylenebis(salicyldene imine)), with a core structure similar to **19** ($U = 55$ cm^{-1}, $T_B = 3$ K).[98] The weak performances of SMMs involving heavy metals are because of the lack of strong magnetic axiality of the latter due to their relatively small spin and low site symmetry in polynuclear complexes.

4.1. Ln-based polynuclear SMMs

The only metal ions that can maintain a high magnetic axiality of their doublet ground state in a low-symmetry environment are lanthanides.[79] Therefore, they are the best candidates for designing polynuclear SMMs. However, they face the problem of highly localized 4f orbitals, resulting in very small exchange interactions between the paramagnetic centers. As in the cases of heavy TM and actinides, the Ln core should be connected to high-spin 3d metal ions, a strategy that is additionally motivated by the much stronger exchange interactions in mixed Ln–M complexes than in pure lanthanide polynuclear complexes.[99] Figure 7a shows that the use of $S = 3/2$ TM ions exchange-coupled to Dy^{III} (Dy_2Cr_2, **21**, $[Cr_2Dy_2(OMe)_2(O_2CPh)_4(mdea)_2(NO_3)_2]$, where $mdeaH_2$ is N-methyldiethanolamine) results in a magnetization blocking that is greater than that of heavy TM and actinide SMMs ($U = 54$ cm^{-1}, $T_B = 3.5$ K),[100] which is further

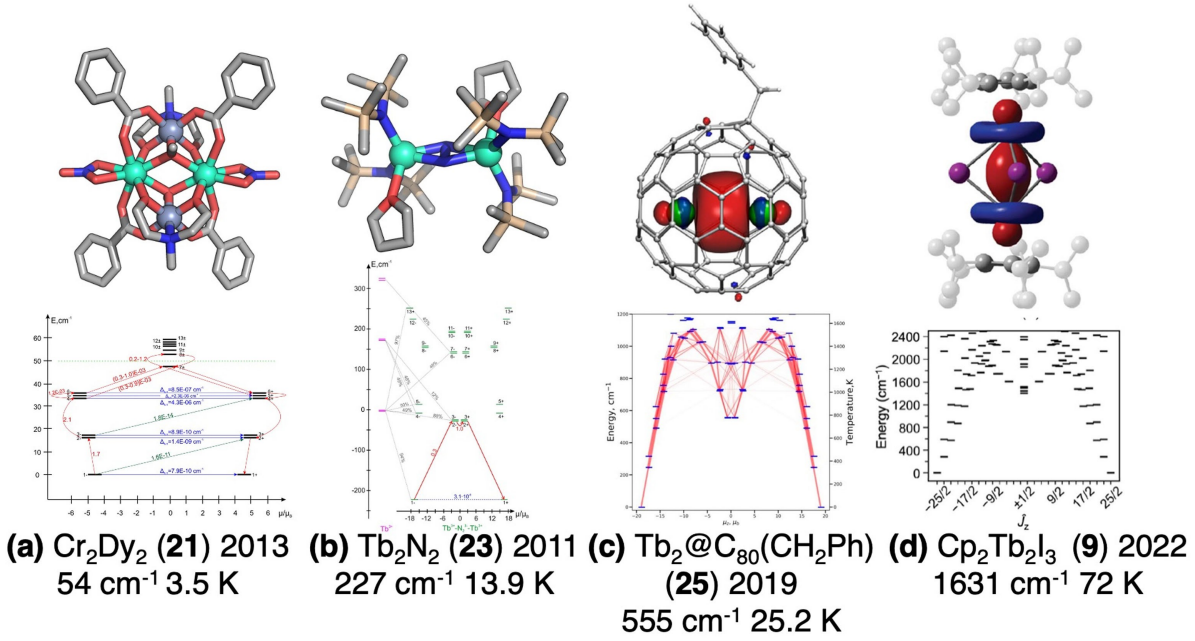

Figure 7. Molecular structures and the low-lying exchange spectrum of selected families of mixed Ln-based compounds, with the year, energy barrier and T_B indicated. (a) Dy_2Cr_2 (**21**).[100] Copyright 2013 Wiley-VCH. (b) $\{[(Me_3Si)_2N]_2(THF)Ln\}_2(\mu\text{-}N_2)^{3-}$ (**23**).[103] Copyright 2011 American Chemical Society. (c) $Ln_2@C_{80}(CH_2Ph)$ (**25**).[107] Copyright 2018 Springer Nature. (d) $Cp_2Tb_2I_3$ (**9**).[27] Copyright 2018 American Association for the Advancement of Science. The last two systems show a singly occupied Ln–Ln bonding molecular orbital. All the atoms are represented by sticks, while the metals are represented by balls. Gray, red, blue, light brown and purple sticks correspond to carbon, oxygen, nitrogen, silicon and iodine atoms, respectively, while the gray and light green balls correspond to the chromium and lanthanide cations, respectively.

increased by replacing them with $S=5/2$ ones such as Fe^{III}. The important point is the magnetic isotropy of the 3d metal ions, since the ZFS of their spin decreases magnetization blocking.[101]

Another approach employed for increasing blocking temperatures is based on the application of strong exchange coupling between metal ions and radicals or free electrons, which might help suppress unwanted spin relaxation processes. In 2011, it was demonstrated that the inclusion of a radical bridge (N_2^{3-}) can give rise to strong antiferromagnetic Ln-radical coupling and a high blocking temperature. The first described dinuclear Dy^{III} compound (**22**, $[K(18\text{-crown-6})]\{[(Me_3Si)_2N]_2(THF)Dy\}_2(N_2))$[102] was shown to have a blocking barrier of 123 cm^{-1} and a blocking temperature of 8.3 K, which was quickly surpassed by its analogous Tb^{III} compound that presented a T_B of 13.9 K (**23**, $[K(18\text{-crown-6})(THF)_2]\{[(Me_3Si)_2N]_2(THF)Tb\}_2(N_2)$, Figure 7b).[103] Theoretical studies combining DFT and CASSCF calculations have shown the dominant contribution of the kinetic mechanism to the exchange coupling as well as the importance of the admixture of excited CF states to the ground state in Ln via the exchange interaction and to the fact that a strong exchange interaction can also be detrimental to the barrier if the axiality is diminished due to it.[116] Other radical ligands have been tested as well.[104] However, the T_B record (20 K) in this type of compounds is still held by the N_2^{3-} radical-bridged dinuclear complex, but with a different Ln coordination (**24**, $[K(crypt\text{-}222)][(Cp^{Me4H}{}_2Tb)_2(N_2)]$where Cp^{Me4H} is tetramethylcyclopentadienyl).[105] It can be postulated that the anisotropy and the exchange coupling are maximized by the change in the Tb coordination. However, theoretical results have shown the importance of the CF generated by the N_2^{3-} radical bridge (due to the large electrostatic and covalent effects) and that the almost perpendicular alignment of the Cp ligands with respect to N_2^{3-} reduces Tb anisotropy. Different outer radical bridging ligands have been proposed to improve SMM behavior.[106]

Additionally, a different approach has been pursued that is based on Ln–Ln bonds, a field that is still emerging. Metal-metal bonds require diffuse valence orbitals, which are elusive in Ln^{III} complexes due to the localized nature of the 4f orbitals. However, single-electron Ln–Ln bonds can be formed through the contribution of 6 s or 5d orbitals. The first examples involving the method based on Ln–Ln bonds took advantage of the restricted space inside a fullerene to couple two Ln ions and obtain a strong interaction between them.[108–110] There are several examples of endohedral dimetallofullerenes where strong coupling arises from the existence of a single-electron Ln–Ln σ-bond with a 6 s-orbital parentage (see Figure 7c). In these systems, there is a delocalization of an unpaired electron between the Ln^{III} ions [Ln^{III}-e-Ln^{III}], which results in a strong ferromagnetic coupling between the lanthanide ions. However, the strong coupling is not the only relevant component, with the ion anisotropy and collinearity of the Ln spins also being crucial. As a result, the $Tb_2@C_{80}(CH_2Ph)$ compound (**25**) holds the T_B record in this family of compounds (25.2 K).[107]

Using this family of compounds and to increase the chemistry of the Ln–Ln metal bonds, a mixed-valence

$Ln^{III}Ln^{II}$ $Cp_2Ln_2I_3$ compound (Ln=Tb and Dy, corresponding to **8** and **9**, respectively) was developed by a one-electron reduction of the dinuclear analogous Ln^{III}_2 complex.[27] This compound also exhibits a valence delocalization due to a single-electron σ-bond with a dz^2-orbital parentage (see Figure 7d), resulting in the [Ln^{III}-e-Ln^{III}] system. The strong ferromagnetic exchange interaction between the Ln ions is induced by a Hund coupling of the delocalized electron (e) to both Ln ions, an effect called double-exchange[111] that is well known in the magnetism of mixed-valence complexes. These compounds show a different chemical strategy for the achievement of a huge coercive magnetic field (14 T at 60 K in the Tb system, **9**). However, they do not display a higher U and T_B than the best mononuclear Ln-based SMMs (Figure 4). In mixed-valence dilanthanides, as well as in the radical-bridged one (Figure 7b), the height of the blocking barrier is determined by the reversal of magnetization on a single metal ion, i.e., by its own blocking barrier and/or by the exchange interaction with a neighboring radical/lanthanide.[116] This explains why magnetization blocking does not increase if more magnetic centers are coupled in a chain, an effect well known among single-chain magnets.[112] In such systems, the finite and infinite models lead to approximately similar results for the dynamic magnetic properties, with no significant changes for either ferromagnetic[113] or antiferromagnetic[114] couplings between the magnetic centers.

4.2. Prospects for efficient polynuclear SMMs

The early strategy in SMM research was to design complexes with a large total spin S that involved a large number of magnetic centers (Figure 1a–c). The rationale behind this approach was the generic expression for the height of the barrier in spin complexes with axial magnetic anisotropy, $U=|D|S^2$ $(D<0)$.[11–14] Besides a high S, this relationship also suggests a large value of the axial ZFS parameter D that is achieved, in particular, for the parallel alignment of local main anisotropy axes.[115] It was previously argued, however, that $|D|$ strongly decreases with the total spin of the complex,[89] with the height of the blocking barrier not generally rising with S, leading to the conclusion that the sign of the exchange interaction between the magnetic centers in SMMs is unimportant. However, this conclusion does not apply to many cases, especially systems with a large number of magnetic sites. As an example, consider an arbitrary system containing N magnetic centers with equal spins (S_i) as well as equal axial ZFS parameters (D_i) and parallel anisotropy axes (Figure 8a–c). In a ferromagnetic state corresponding to the maximal total spin, $S=S_m$, for the limit $S_m \gg 1$ the blocking barrier $U_{Sm} \approx |D_i|(S_i-1/2)S_m$,[89a] which, due to the relation $S_m=NS_i$, scales with the number of magnetic centers, a fact that is well known for ferromagnetic nanoparticles.[129] The above relationship can be rewritten in the form $(|D_i|S_i^2)$ $(1–1/2S_i)$ N, which

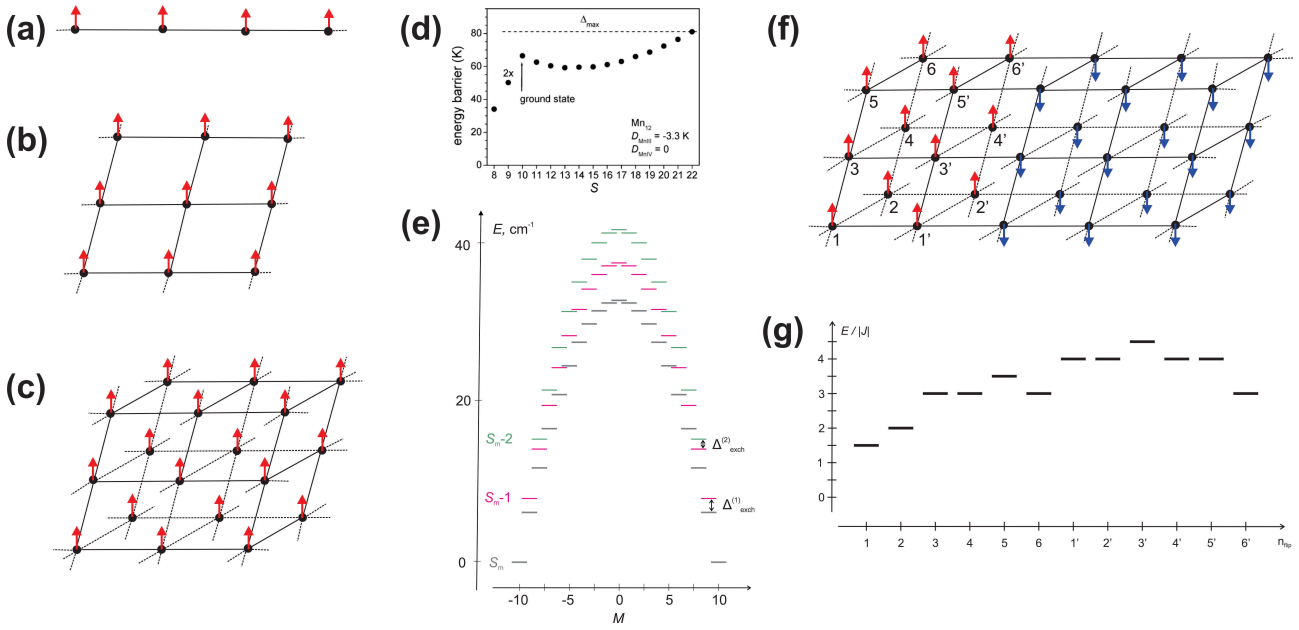

Figure 8. (a–c) Regular ferromagnetic networks of three dimensionalities; the spins on the magnetic sites are aligned to local main anisotropy axes. (d) Height of U_S of the lowest spin terms for each value of $S \geq 8$ ($S_m=22$) in Mn_{12}-acetate.[89a] Copyright 2007 American Chemical Society. (e) Blocking barriers for three different spin terms in a regular ferromagnetic network, with a Heisenberg exchange interaction for $N=5$, $S_i=2$ ($S_m=10$) and $D_i=-2.5$ cm^{-1}. Only one term for $S=S_m-1$ and $S=S_m-2$ is shown. The height of the barrier for each excited spin term is smaller by $|D_i|(S_i-1/2)=3.75$ cm^{-1} than the previous one, while the entire barrier is shifted up by the corresponding exchange energy. The interactions between the excited spin terms induced by the ZFS on the sites is neglected for simplicity, causing the corresponding barriers to have a perfect parabolic shape. (f) Magnetic configuration corresponding to the top of the blocking barrier in a regular ferromagnetic network, with an Ising exchange interaction $(-|J|S_{iz}S_{jz})$ between the ground spin-orbit doublets ($S_i=1/2$) at the nearest neighboring sites. (g) Variation of the energy of the regular Ising network in (f) with respect to its ferromagnetic ground state after consecutive flips of magnetic moments on the magnetic sites 1–6 of the first layer and 1′–6′ of the second layer (see (f) for the numeration of the flipping sites).

indicates that for a fixed N and on-site ZFS ($|D_i|S_i^2$), the blocking barrier increases with the value of the local spins S_i. The barrier corresponding to the non-ferromagnetic state $S=S_m-1$ will be lower by the quantity $U_{Sm}-U_{Sm\text{-}1}=|D_i|(S_i-1/2)$, suggesting that U_S decreases linearly with a diminishing S. This is also observed in non-regular magnetic systems, such as Mn_{12}-acetate, for spin values close to the ferromagnetic one (Figure 8d). Therefore, the sign of the exchange interaction between the magnetic centers is important for SMM performance, with the highest blocking barrier achieved for the ferromagnetic ground state.

These results apply to complexes with a Heisenberg exchange interaction between magnetic sites, presenting eigenstates $|SM>$ characterized by a definite total spin and its projection (SMMs of type I). In the presence of axial magnetic anisotropy on sites with parallel local main magnetic axes, the total spin projections M in their directions ($M=-S_m, \ldots S_m$) are still good quantum numbers. On the contrary, S will not be conserved anymore, implying that the $|SM>$ states with the same value of M and different S values will be intermixed by the axial magnetic anisotropy. An exception are ferromagnetic states $|S_mM>$ that remain eigenstates in the presence of an axial ZFS on the sites if the latter are equivalent. Accordingly, the value of U_{Sm} is not affected by the exchange interaction, while the shape of this barrier remains perfectly parabolic (Figure 8e). Furthermore, in sufficiently large complexes, the conservation of M quenches the magnetization reversing transitions for most pairs of states on the two sides of this barrier due to the very large difference in their momenta ($\Delta M=M_2-M_1 \gg 1$), thus making the S_m-barrier completely opaque unless the levels close to its top become thermally populated. A similar situation occurs for other barriers with large values of S (Figure 8e). However, due to their rapidly increasing number with decreasing S values ($N_{Sm\text{-}1}=N$-1, $N_{Sm\text{-}2}=N(N$-1)/2, …) and a quadratic dependence of the number of the spin-flip transitions on the number of thermally available U_S, the effective blocking barrier will be much lower than the U_{Sm}. To reduce the density of S terms in the thermally accessible energy domain, the exchange interaction between the sites should be as large as possible, while the magnetic network should be three-dimensional (Figure 8c). Moreover, the density of low-lying S terms quickly declines with a decreasing N, which means that there is a preference for S_i to be large ($S_m=NS_i$). Relatively large ionic anisotropy in combination with $S_i=2$ is observed in complexes of Fe^{II} and Co^{III},[117] although a strong ferromagnetic exchange interaction is not easily achieved for these metal ions. An alternative solution would be the use of ferrimagnetic regular systems such as the Prussian blue TM cubic networks exhibiting a very large exchange interaction between the metal sites.[118] However, the ground state spin in ferrimagnetic systems ($S_{ferri}<S_m$) involves a much higher density of spin terms in the low-energy domain than in ferromagnetic complexes. We may conclude that the main advantage of the ferromagnetic ground state in a polynuclear SMM is not so much the increase in the height of the low-lying blocking barriers, but the decrease in the density of the thermally accessible S terms.

Heisenberg exchange occurs between metal centers with a quenched orbital momentum. When the latter becomes (partly) unquenched, an Ising exchange interaction can develop along with the Heisenberg one in the presence of high axial symmetry on the metal sites (SMMs of type II). The total momentum projection M along the Ising axis (z) is again good quantum number if the polynuclear compound is regular, also in the presence of axial ionic anisotropy on the sites. The conservation of M gives rise to strong magnetization blocking, like in the Heisenberg complexes, but the nature of the blocking barriers is different. Thus, in pure Ising complexes, the barrier of the reversal of magnetization consists of steps of different Ising exchange levels (Figure 8g) and not of $(2S+1)$ ZFS components of the one exchange S term. Moreover, the top of the barrier corresponds to the energy of the "domain wall" between two ferromagnetically ordered parts of opposite magnetization (Figure 8f), thus involving only the centers from the smallest cross-section of the regular structure. This is contrary to Heisenberg systems, where the top of the barrier corresponds to the half-spin reversal on all magnetic centers. Thus, to achieve the same height of the barrier, polynuclear SMMs of the Ising type require many more magnetic sites. Figure 8f also suggests that the best shape for the Ising systems is cubic. The main drawback of such SMMs is a weak exchange coupling, since a three-dimensional Ising interaction is only obtained for lanthanide and actinide ions, amounting to a few cm^{-1}. The ferrimagnetic Ising interaction is one order of magnitude larger for mixed lanthanide-TM compounds[100] and two orders of magnitude larger in lanthanide-radical complexes.[102,103] However, no networks of this type have been reported to date. For ferrimagnetic Ising systems, the top of the lowest blocking barrier will be again determined by a domain wall, as in the ferromagnetic case (Figure 8f), which separates two ferrimagnetic Ising orders of opposite directions. However, contrary to the SMMs of the Heisenberg type, other relaxation paths will always pass higher than this lowest barrier. The latter will increase linearly with the strength of the Ising exchange interaction and the number of magnetic centers in the smallest cross-section of the magnetic structure, unlike in Heisenberg complexes, where the rise of the effective blocking barrier and T_B are likely to reach saturation for a large number of magnetic ions.

5. Ln Ions on Surfaces

Single Ln ions deposited on surfaces represent the limit of the miniaturization of memory storage devices.[119] They have been already used for testing various magnetic recording techniques at the atomic scale.[120] Different procedures for placing magnetic systems on surfaces have been addressed,[121] such as using active surfaces like silicon oxide that can coordinate lanthanide cations directly,[122] substituting ligands from a complex, or producing a hybrid coordination of the metal.[123] An interesting option is to use an ionic support, e.g., MgO, to deposit the metal ions in order to reduce the surface vibrations that can generate spin

relaxation.[124] The magnetic anisotropy of deposited lanthanide ions arises from the CF splitting of the ground J multiplet induced by its chemical binding to a surface atom.[125] Although magnetic relaxation proceeds via the same mechanisms as those for magnetic molecules in crystals [Eq. (1)], the crucial difference is that the lanthanide ions on surfaces, being impurity systems, interact with the local vibrations rather than the extended phonons. The local vibrations show up in the projected density of the phonon states (pDOS) as narrow Gaussian distributions. Thus, Figure 9a shows the local vibrations corresponding to the in-plane and out-of-plane displacements of an Ho atom deposited on the MgO surface.[124] The former are active vibrations since they induce the main electron-phonon coupling between the CF doublets. The pDOS for these vibrations is centered at around 34 cm^{-1}, which does not match any excitation energy for the low-lying doublets of the Ho^{2+} cation. Hence, all the relaxation mechanisms in Equation (1) involving the ground and low-lying doublet excited states will be blocked except for the second-order Raman via these local vibrations [third term in Eq. (1)]. The latter resembles the Orbach process at low temperatures, $\tau^{-1}=\tau_0^{-1}\ \exp(-\hbar\omega/kT)$, with $\hbar\omega$ corresponding to the frequency of the localized vibration (the center of the corresponding pDOS) and the prefactor $\tau_0=60$ s exceeding the usual Orbach prefactors by many orders of magnitude. This results in a very strong magnetization blocking of hundreds of seconds at 35 K, which extends to 45 K when an external field is applied (Figure 9c).[126] The latter is explained by the suppression of this Raman mechanism when a bias field overcomes the width of the pDOS for these localized vibrations (Figure 9b). Taking into account the realistic width of the pDOS in modeling the relaxation[53] is crucial for the description of $\tau(H)$, a feature not included for simplicity in the third term of Equation (1), which instead considers the vanishing width of the pDOS and a zero-applied field.

We may conclude that Ho/MgO offers a third scenario of magnetization blocking that crucially differs from that of the weakly and strongly axial SMMs since it does not require strong magnetic axiality within the spin-orbit doublets. One might expect that imposing it by using, e.g., dysprosium ions would suppress the remaining weak relaxation channels. Investigations have shown that Dy^{III}/MgO blocks magnetization for days at $T=1$ K (outperforming all known mononuclear SMMs). However, the blocking decreases rapidly with increasing temperature.[120] This suggests a non-negligible role of MgO phonons in the relaxation process via the first doublet excited state, which is not as strongly axial as in many Ln-based mononuclear SMMs shown in Figure 4. Despite a resemblance to [LnO] diatomic systems, the lanthanide ions in Ln/MgO actually experience a strong CF of a four-fold symmetry, reducing their magnetic axiality. The situation might be improved by depositing LnO units on the MgO surface. Calculations show that $[DyO]^+$ vertically coordinated to MgO (Figure 9d) gives a barrier of around 4000 cm^{-1} at 2.3 Å from the surface.[59] The increase in U compared to that for the respective diatomics is due to an additional axial CF contribution from the surface oxygen atom, similar to other compounds with a linear OLnO core.[74] Such a coordination mode, however, is hardly encountered in real systems, with a parallel coordination to the surface being more realistic (Figure 9e).[65] Despite the lack of symmetry in such a coordination, the barrier still remains very high because of the much stronger bonding within the LnO unit compared to its coupling to the surface.

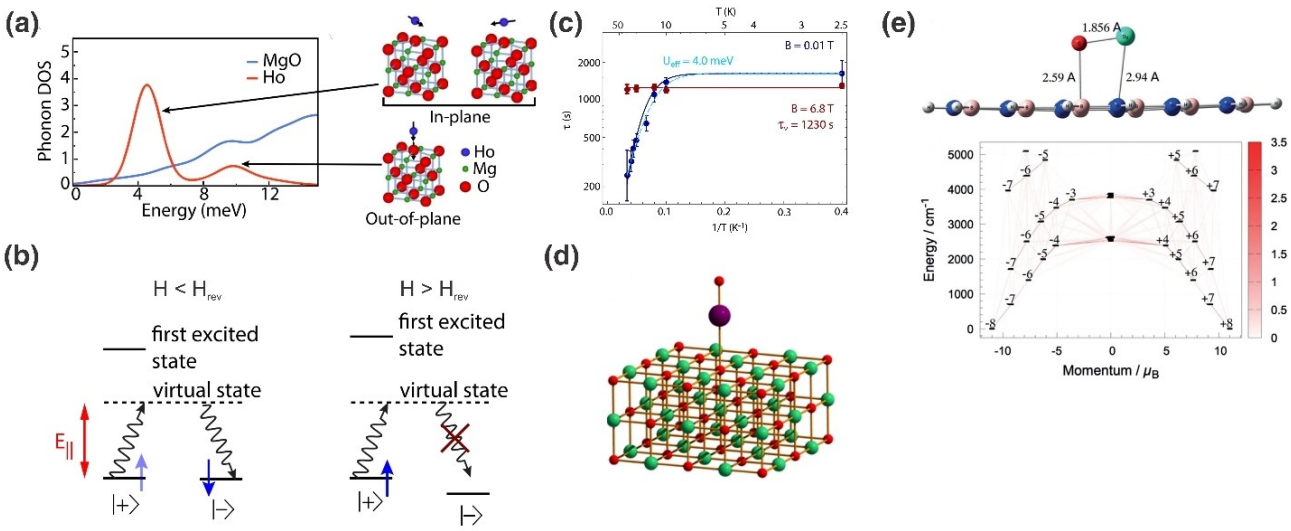

Figure 9. (a) The pDOS for three local vibrational modes of Ho/MgO. (b) Mechanisms of relaxation via the active local vibrations in Ho/MgO. (c) Relaxation time $\tau(T)$ for Ho/MgO with and without the applied field (B) extracted from XMCD spectroscopy.[124] Copyright 2020 American Physical Society. Due to sample irradiation during the measurements, the obtained value of τ at a low temperature (constant domain) is $1 \div 2$ orders of magnitude lower than that observed in the STM experiments.[126] (d) Ideal coordination of a diatomic LnO to the surface.[59] Copyright 2016 American Chemical Society. (e) A DFT-optimized structure of [DyO]/h-BN and the ab initio calculated multiplet structure displaying a $U > 2000$ cm^{-1}.[65] Copyright 2020 Wiley-VCH.

6. Summary and Outlook

We have discussed several approaches for the design of magnetic complexes exhibiting high magnetization blocking. The two basic requirements for efficient SMMs are: (i) the presence of many spin-orbit doublets with definite angular momentum projections (M,-M) in their two components and (ii) strong energy separation between the doublets, with the low-lying ones being characterized by the largest M values. For such multiplets, the magnetization reversing transitions are suppressed at a low temperature, so that the flip of magnetization of the complex basically occurs via a thermal population of the high-lying doublets with lower M values. These requirements are met by the design of ligand environments that provide high magnetic axiality and large CF separation of the spin-orbit doublets on the metal ions. Another favorable factor for magnetization blocking is the lack of efficiently coupled vibrations/phonons that could induce transitions between the magnetic levels. While the first strategy is well understood and already accounted for in the synthesis of new SMMs, the second one is largely uncontrollable. At the same time, it is important to understand how far the existing or prospective compounds stay from real applications as memory units.

To safely store data for years at a temperature T, a classical anisotropy barrier should present a $U \geq 60\, k_B T$.[119] In liquid nitrogen (77 K), the height of such a barrier should reach 3200 cm^{-1}, which is not attainable in current SMMs, but is well within the reach of diatomic lanthanides that are vertically deposited onto a surface (Figure 9d), which is, unfortunately, an unrealistic coordination scenario. On the other hand, the synthesis of mononuclear Ln-based SMMs, with a blocking barrier around two-fold greater than that of existing compounds (Figure 4), is in principle possible by using inverted CF ligands in the equatorial plane that could provide at least half of the strength of the axial CF given by the apical ligands. One should bear in mind, however, that in molecular systems, the barrier is not classic and the under-barrier transitions cannot be eliminated completely (Figure 3d). To reduce them, a strategy inspired by the Ho/MgO example (Figure 9), in which the relaxation process takes place via local vibrations, could be used. The main problem with the deposition of polyatomic SMMs on surfaces is their general loss of symmetry, which strongly reduces the T_B.[121]

To store information at room temperature, a blocking barrier of around 12000 cm^{-1} is required, which is in principle not achievable in mononuclear complexes. Numerous polynuclear SMMs synthesized to date show a discouraging trend of U and T_B not increasing with the number of magnetic ions, even in complexes containing 84 metal ions (**4**, Figure 1). A clear solution would be the synthesis of regular polynuclear complexes with equivalent magnetic sites, i.e., with parallel local anisotropy/main magnetic axes and intersite exchange interactions. As discussed above, such complexes should be either of the ferromagnetic Heisenberg type (with axial magnetic anisotropy on the sites) or of the ferrimagnetic Ising type, with very strong intersite exchange interactions in both cases. Attempts to construct anisotropic 3D magnetic networks using cyano-bridged bimetallic ferromagnets synthesized from the $[Mo(CN)_7]^{4-}$ precursor have shown a Curie temperature of several tens of K and weak anisotropy[127] due to the low site symmetry of the precursor. The best source of intrasite magnetic anisotropy would be Ln ions capable of giving strong axial anisotropy in the absence of site symmetry. To provide strong Ising exchange interactions, they should be coupled to isotropic transition metals or radicals. For polynuclear SMMs of the Heisenberg type, the main problem is achieving strong ferromagnetic exchange interactions with all the neighbors. Besides three-dimensionality and regularity combined with strong magnetic axiality on the metal sites (conditions not yet paid attention to in the synthesis of SMMs), the growth of such networks might be quenched by techniques used to produce synthetic nanoparticles.[128] Under these conditions, barriers are expected to be reached for room temperature operation involving several hundred Ln–R units if the synthesis of suitable lanthanide-radical networks becomes affordable. Such regular magnetic complexes are still much smaller than the typical magnetic nanoparticles, amounting to tens to a hundred thousand metal ions.[129]

Acknowledgements

ER and SGC thank the Spanish Ministerio de Ciencia e Innovación (the PID2021-122464NB-I00, TED2021-129593B-I00 and Maria de Maeztu CEX2021-001202-M grants) and the Generalitat de Catalunya (2021 SGR 00286 grant) and ER also acknowledges the Generalitat de Catalunya for an ICREA Academia grant.

Conflict of Interest

The authors declare no conflict of interest.

Data Availability Statement

Data sharing is not applicable to this article as no new data were created or analyzed in this study.

Keywords: Lanthanide Complexes · Magnetization Blocking · Memory Devices · Single-Molecule Magnets · Transition-Metal Complexes

[1] R. Sessoli, H. L. Tsai, A. R. Schake, S. Y. Wang, J. B. Vincent, K. Folting, D. Gatteschi, G. Christou, D. N. Hendrickson, *J. Am. Chem. Soc.* **1993**, *115*, 1804–1816.
[2] R. Sessoli, D. Gatteschi, A. Caneschi, M. A. Novak, *Nature* **1993**, *365*, 141–143.
[3] M. N. Leuenberger, D. Loss, *Nature* **2001**, *410*, 789–793.
[4] L. Bogani, W. Wernsdorfer, *Nat. Mater.* **2008**, *7*, 179–186.
[5] M. Mannini, F. Pineider, P. Sainctavit, C. Danieli, E. Otero, C. Sciancalepore, A. M. Talarico, M.-A. Arrio, A. Cornia, D. Gatteschi, R. Sessoli, *Nat. Mater.* **2009**, *8*, 194–197.

[6] A. Gaita-Ariño, F. Luis, S. Hill, E. Coronado, *Nat. Chem.* **2019**, *11*, 301–309.
[7] M. Atzori, R. Sessoli, *J. Am. Chem. Soc.* **2019**, *141*, 11339–11352.
[8] P. Stano, D. Loss, *Nat. Rev. Phys.* **2022**, *4*, 672–688.
[9] E. Moreno-Pineda, W. Wernsdorfer, *Nat. Rev. Phys.* **2021**, *3*, 645–659.
[10] E. Coronado, *Nat. Rev. Mater.* **2019**, *5*, 87–104.
[11] D. Gatteschi, R. Sessoli, J. Villain, *Molecular Nanomagnets*, Oxford University Press, Oxford **2006**.
[12] A. Zabala-Lekuona, J. M. Seco, E. Colacio, *Coord. Chem. Rev.* **2021**, *441*, 213984.
[13] Y.-C. Chen, M.-L. Tong, *Chem. Sci.* **2022**, *13*, 8716–8726.
[14] S. T. Liddle, J. van Slageren, *Chem. Soc. Rev.* **2015**, *44*, 6655–6669.
[15] R. Sessoli, A. K. Powell, *Coord. Chem. Rev.* **2009**, *253*, 2328–2341.
[16] J. Tang, P. Zhang, *Lanthanide Single Molecule Magnets*, Springer Berlin Heidelberg, Berlin **2015**.
[17] C. J. Milios, A. Vinslava, W. Wernsdorfer, S. Moggach, S. Parsons, S. P. Perlepes, G. Christou, E. K. Brechin, *J. Am. Chem. Soc.* **2007**, *129*, 2754–2755.
[18] A. M. Ako, I. J. Hewitt, V. Mereacre, R. Clérac, W. Wensdorfer, C. E. Anson, A. K. Powell, *Angew. Chem. Int. Ed.* **2006**, *45*, 4926–4929.
[19] A. J. Tasiopoulos, A. Vinslava, W. Wernsdorfer, K. A. Abboud, G. Christou, *Angew. Chem. Int. Ed.* **2004**, *43*, 2117–2121.
[20] J. Cirera, E. Ruiz, S. Alvarez, F. Neese, J. Kortus, *Chem. Eur. J.* **2009**, *15*, 4078–4087.
[21] N. Ishikawa, M. Sugita, T. Ishikawa, S.-y. Koshihara, Y. Kaizu, *J. Am. Chem. Soc.* **2003**, *125*, 8694–8695.
[22] A. G. Martynov, Y. Horii, K. Katoh, Y. Bian, J. Jiang, M. Yamashita, Y. G. Gorbunova, *Chem. Soc. Rev.* **2022**, *51*, 9262–9339.
[23] D. E. Freedman, W. H. Harman, T. D. Harris, G. J. Long, C. J. Chang, J. R. Long, *J. Am. Chem. Soc.* **2010**, *132*, 1224–1225.
[24] C. A. P. Goodwin, F. Ortu, D. Reta, N. F. Chilton, D. P. Mills, *Nature* **2017**, *548*, 439–442.
[25] F.-S. Guo, B. M. Day, Y.-C. Chen, M.-L. Tong, A. Mansikkamäki, R. A. Layfield, *Science* **2018**, *362*, 1400–1403.
[26] F.-S. Guo, B. M. Day, Y.-C. Chen, M.-L. Tong, A. Mansikkamäki, R. A. Layfield, *Angew. Chem. Int. Ed.* **2017**, *56*, 11445–11449.
[27] C. A. Gould, K. R. McClain, D. Reta, J. G. C. Kragskow, D. A. Marchiori, E. Lachman, E.-S. Choi, J. G. Analytis, R. D. Britt, N. F. Chilton, B. G. Harvey, J. R. Long, *Science* **2022**, *375*, 198–202.
[28] A. Abragam, B. Bleaney, *Electron Paramagnetic Resonance of Transition Ions*, Reprinted ed., Oxford University Press, Oxford **2012**.
[29] J. W. Orton, *Electron Paramagnetic Resonance : An Introduction to Transition Group Ions in Crystals*, Iliffe, London **1968**.
[30] J. H. Van Vleck, *Phys. Rev.* **1940**, *57*, 426–447.
[31] M. Ding, A. K. Hickey, M. Pink, J. Telser, D. L. Tierney, M. Amoza, M. Rouzières, T. J. Ozumerzifon, W. A. Hoffert, M. P. Shores, E. Ruiz, R. Clérac, J. M. Smith, *Chem. Eur. J.* **2019**, *25*, 10625–10632.
[32] L. T. A. Ho, L. F. Chibotaru, *Phys. Rev. B* **2018**, *97*, 024427.
[33] S. S. Eaton, J. Harbridge, G. A. Rinard, G. R. Eaton, R. T. Weber, *Appl. Magn. Reson.* **2001**, *20*, 151–157.
[34] J. G. Castle, D. W. Feldman, *Phys. Rev.* **1965**, *137*, A671–A673.
[35] Y. S. Ding, K. X. Yu, D. Reta, F. Ortu, R. E. P. Winpenny, Y. Z. Zheng, N. F. Chilton, *Nat. Commun.* **2018**, *9*.
[36] S. Mondal, A. Lunghi, *J. Am. Chem. Soc.* **2022**, *144*, 22965–22975.
[37] K. K. P. Srivastava, H. C. Singh, *Phys. Status Solidi B* **1980**, *101*, 43–49.
[38] D. A. Garanin, E. M. Chudnovsky, *Phys. Rev. B* **1997**, *56*, 11102–11118.
[39] M. N. Leuenberger, D. Loss, *Phys. Rev. B* **2000**, *61*, 1286–1302.
[40] F. Habib, P.-H. Lin, J. Long, I. Korobkov, W. Wernsdorfer, M. Murugesu, *J. Am. Chem. Soc.* **2011**, *133*, 8830–8833.
[41] F. Pointillart, K. Bernot, S. Golhen, B. Le Guennic, T. Guizouarn, L. Ouahab, O. Cador, *Angew. Chem. Int. Ed.* **2015**, *54*, 1504–1507.
[42] J. M. Zadrozny, J. Niklas, O. G. Poluektov, D. E. Freedman, *ACS Cent. Sci.* **2015**, *1*, 488–492.
[43] A. Castro-Alvarez, Y. Gil, L. Llanos, D. Aravena, *Inorg. Chem. Front.* **2020**, *7*, 2478–2486.
[44] A. Lunghi, S. Sanvito, *Sci. Adv.* **2019**, *5*, eaax7163.
[45] A. Lunghi, F. Totti, S. Sanvito, R. Sessoli, *Chem. Sci.* **2017**, *8*, 6051–6059.
[46] A. Albino, S. Benci, L. Tesi, M. Atzori, R. Torre, S. Sanvito, R. Sessoli, A. Lunghi, *Inorg. Chem.* **2019**, *58*, 10260–10268.
[47] C. M. Varma, J. Zaanen, K. Raghavachari, *Science* **1991**, *254*, 989–992.
[48] A. Lunghi, F. Totti, R. Sessoli, S. Sanvito, *Nat. Commun.* **2017**, *8*.
[49] J. J. Baldoví, Y. Duan, R. Morales, A. Gaita-Arino, E. Ruiz, E. Coronado, *Chem. Eur. J.* **2016**, *22*, 13532–13539.
[50] L. Escalera-Moreno, J. J. Baldovi, A. Gaita-Arino, E. Coronado, *Chem. Sci.* **2018**, *9*, 3265–3275.
[51] M. Atzori, L. Tesi, S. Benci, A. Lunghi, R. Righini, A. Taschin, R. Torre, L. Sorace, R. Sessoli, *J. Am. Chem. Soc.* **2017**, *139*, 4338–4341.
[52] M. Amoza, L. Maxwell, N. Aliaga-Alcalde, S. Gómez-Coca, E. Ruiz, *Chem. Eur. J.* **2021**, *27*, 16440–16447.
[53] D. L. Mills, *Phys. Rev.* **1966**, *146*, 336–343.
[54] A. N. Bone, C. N. Widener, D. H. Moseley, Z. Liu, Z. Lu, Y. Cheng, L. L. Daemen, M. Ozerov, J. Telser, K. Thirunavukkuarasu, D. Smirnov, S. M. Greer, S. Hill, J. Krzystek, K. Holldack, A. Aliabadi, A. Schnegg, K. R. Dunbar, Z.-L. Xue, *Chem. Eur. J.* **2021**, *27*, 11110–11125.
[55] R. Marx, F. Moro, M. Dörfel, L. Ungur, M. Waters, S. D. Jiang, M. Orlita, J. Taylor, W. Frey, L. F. Chibotaru, J. van Slageren, *Chem. Sci.* **2014**, *5*, 3287–3293.
[56] C. P. Slichter, *Springer Series in Solid-State Sciences*, Springer Berlin Heidelberg, Berlin **1978**.
[57] A. Lunghi, *Sci. Adv.* **2022**, *8*, eabn7880.
[58] H. L. C. Feltham, Y. Lan, F. Klöwer, L. Ungur, L. F. Chibotaru, A. K. Powell, S. Brooker, *Chem. Eur. J.* **2011**, *17*, 4362.
[59] L. Ungur, L. F. Chibotaru, *Inorg. Chem.* **2016**, *55*, 10043–10056.
[60] D. Aravena, E. Ruiz, *Dalton Trans.* **2020**, *49*, 9916–9928.
[61] K. S. Pedersen, J. Dreiser, H. Weihe, R. Sibille, H. V. Johannesen, M. A. Sørensen, B. E. Nielsen, M. Sigrist, H. Mutka, S. Rols, J. Bendix, S. Piligkos, *Inorg. Chem.* **2015**, *54*, 7600–7606.
[62] M. Gregson, N. F. Chilton, A.-M. Ariciu, F. Tuna, I. F. Crowe, W. Lewis, A. J. Blake, D. Collison, E. J. L. McInnes, R. E. P. Winpenny, S. T. Liddle, *Chem. Sci.* **2016**, *7*, 155–165.
[63] D. Gatteschi, R. Sessoli, *Angew. Chem. Int. Ed.* **2003**, *42*, 268–297.
[64] L. Ungur, M. Thewissen, J.-P. Costes, W. Wernsdorfer, L. F. Chibotaru, *Inorg. Chem.* **2013**, *52*, 6328–6337.
[65] W. Zhang, A. Muhtadi, N. Iwahara, L. Ungur, L. F. Chibotaru, *Angew. Chem. Int. Ed.* **2020**, *59*, 12720–12724.

[66] N. Kulikov, L. A. Kaledin, A. I. Kobyliansky, L. V. Gurvich, *Can. J. Phys.* **1984**, *62*, 1855–1870.
[67] P. C. Bunting, M. Atanasov, E. Damgaard-Møller, M. Perfetti, I. Crassee, M. Orlita, J. Overgaard, J. van Slageren, F. Neese, J. R. Long, *Science* **2018**, *362*, eaat7319.
[68] J. M. Zadrozny, D. J. Xiao, M. Atanasov, G. J. Long, F. Grandjean, F. Neese, J. R. Long, *Nat. Chem.* **2013**, *5*, 577–581.
[69] J. S. Griffith, *The theory of transition-metal ions*, University Press, Cambridge **1961**.
[70] S. Gómez-Coca, E. Cremades, N. Aliaga-Alcalde, E. Ruiz, *J. Am. Chem. Soc.* **2013**, *135*, 7010–7018.
[71] V. S. Mironov, L. F. Chibotaru, A. Ceulemans, *J. Am. Chem. Soc.* **2003**, *125*, 9750–9760.
[72] M. V. Bennett, J. R. Long, *J. Am. Chem. Soc.* **2003**, *125*, 2394–2395.
[73] E. Cremades, E. Ruiz, *Inorg. Chem.* **2011**, *50*, 4016–4020.
[74] S. Gómez-Coca, D. Aravena, R. Morales, E. Ruiz, *Coord. Chem. Rev.* **2015**, *289–290*, 379–392.
[75] F. Neese, E. I. Solomon, *Magnetism: Molecules to Materials, Vol. 4* (Eds.: J. S. Miller, M. Drillon), Wiley-VCH, Weinheim **2003**, p. 345.
[76] X.-N. Yao, J.-Z. Du, Y.-Q. Zhang, X.-B. Leng, M.-W. Yang, S.-D. Jiang, Z.-X. Wang, Z.-W. Ouyang, L. Deng, B.-W. Wang, S. Gao, *J. Am. Chem. Soc.* **2017**, *139*, 373–380.
[77] J. M. Zadrozny, M. Atanasov, A. M. Bryan, C.-Y. Lin, B. D. Rekken, P. P. Power, F. Neese, J. R. Long, *Chem. Sci.* **2013**, *4*, 125–138.
[78] K. R. Meihaus, J. R. Long, *Dalton Trans.* **2015**, *44*, 2517–2528.
[79] L. Ungur, L. F. Chibotaru, *Phys. Chem. Chem. Phys.* **2011**, *13*, 20086–20090.
[80] R. J. Blagg, L. Ungur, F. Tuna, J. Speak, P. Comar, D. Collison, W. Wernsdorfer, E. J. L. McInnes, L. F. Chibotaru, R. E. P. Winpenny, *Nat. Chem.* **2013**, *5*, 673–678.
[81] D. Aravena, E. Ruiz, *Inorg. Chem.* **2013**, *52*, 13770–13778.
[82] L. Ungur, L. F. Chibotaru, *Lanthanides and Actinides in Molecular Magnetism*, Wiley-VCH, Weinheim **2015**, pp. 153–184.
[83] Y.-S. Ding, N. F. Chilton, R. E. P. Winpenny, Y.-Z. Zheng, *Angew. Chem. Int. Ed.* **2016**, *55*, 16071–16074.
[84] J. Long, A. O. Tolpygin, E. Mamontova, K. A. Lyssenko, D. Liu, M. D. Albaqami, L. F. Chibotaru, Y. Guari, J. Larionova, A. A. Trifonov, *Inorg. Chem. Front.* **2021**, *8*, 1166–1174.
[85] K. Randall McClain, C. A. Gould, K. Chakarawet, S. J. Teat, T. J. Groshens, J. R. Long, B. G. Harvey, *Chem. Sci.* **2018**, *9*, 8492–8503.
[86] J. C. Vanjak, B. O. Wilkins, V. Vieru, N. S. Bhuvanesh, J. H. Reibenspies, C. D. Martin, L. F. Chibotaru, M. Nippe, *J. Am. Chem. Soc.* **2022**, *144*, 17743–17747.
[87] N. F. Chilton, C. A. P. Goodwin, D. P. Mills, R. E. P. Winpenny, *Chem. Commun.* **2015**, *51*, 101–103.
[88] J. D. Rinehart, J. R. Long, *Chem. Sci.* **2011**, *2*, 2078–2085.
[89] a) O. Waldmann, *Inorg. Chem.* **2007**, *46*, 10035–10037; b) E. Ruiz, J. Cirera, J. Cano, S. Alvarez, C. Loose, J. Kortus, *Chem. Commun.* **2008**, 52–54.
[90] A. Chiesa, F. Cugini, R. Hussain, E. Macaluso, G. Allodi, E. Garlatti, M. Giansiracusa, C. A. P. Goodwin, F. Ortu, D. Reta, J. M. Skelton, T. Guidi, P. Santini, M. Solzi, R. De Renzi, D. P. Mills, N. F. Chilton, S. Carretta, *Phys. Rev. B* **2020**, *101*, 174402.
[91] Y.-C. Chen, J.-L. Liu, L. Ungur, J. Liu, Q.-W. Li, L.-F. Wang, Z.-P. Ni, L. F. Chibotaru, X.-M. Chen, M.-L. Tong, *J. Am. Chem. Soc.* **2016**, *138*, 2829–2837.
[92] Z. Zhu, C. Zhao, T. Feng, X. Liu, X. Ying, X.-L. Li, Y.-Q. Zhang, J. Tang, *J. Am. Chem. Soc.* **2021**, *143*, 10077–10082.
[93] R. Hoffmann, S. Alvarez, C. Mealli, A. Falceto, T. J. Cahill III, T. Zeng, G. Manca, *Chem. Rev.* **2016**, *116*, 8173–8192.
[94] R. C. Walroth, J. T. Lukens, S. N. MacMillan, K. D. Finkelstein, K. M. Lancaster, *J. Am. Chem. Soc.* **2016**, *138*, 1922–1931.
[95] K. Qian, X.-C. Huang, C. Zhou, X.-Z. You, X.-Y. Wang, K. R. Dunbar, *J. Am. Chem. Soc.* **2013**, *135*, 13302–13305.
[96] D.-Q. Wu, D. Shao, X.-Q. Wei, F.-X. Shen, L. Shi, D. Kempe, Y.-Z. Zhang, K. R. Dunbar, X.-Y. Wang, *J. Am. Chem. Soc.* **2017**, *139*, 11714–11717.
[97] V. Hoeke, A. Stammler, H. Bögge, J. Schnack, T. Glaser, *Inorg. Chem.* **2014**, *53*, 257–268.
[98] L. Chatelain, J. P. S. Walsh, J. Pécaut, F. Tuna, M. Mazzanti, *Angew. Chem. Int. Ed.* **2014**, *53*, 13434–13438.
[99] J. Tang, I. Hewitt, N. T. Madhu, G. Chastanet, W. Wernsdorfer, C. E. Anson, C. Benelli, R. Sessoli, A. K. Powell, *Angew. Chem. Int. Ed.* **2006**, *45*, 1729–1733.
[100] S. K. Langley, D. P. Wielechowski, V. Vieru, N. F. Chilton, B. Moubaraki, B. F. Abrahams, L. F. Chibotaru, K. S. Murray, *Angew. Chem. Int. Ed.* **2013**, *52*, 12014–12019.
[101] V. Vieru, T. D. Pasatoiu, L. Ungur, E. Suturina, A. M. Madalan, C. Duhayon, J.-P. Sutter, M. Andruh, L. F. Chibotaru, *Inorg. Chem.* **2016**, *55*, 12158–12171.
[102] J. D. Rinehart, M. Fang, W. J. Evans, J. R. Long, *Nat. Chem.* **2011**, *3*, 538–542.
[103] J. D. Rinehart, M. Fang, W. J. Evans, J. R. Long, *J. Am. Chem. Soc.* **2011**, *133*, 14236–14239.
[104] S. Demir, I.-R. Jeon, J. R. Long, T. D. Harris, *Coord. Chem. Rev.* **2015**, *289–290*, 149–176.
[105] S. Demir, M. I. Gonzalez, L. E. Darago, W. J. Evans, J. R. Long, *Nat. Commun.* **2017**, *8*, 2144.
[106] G. T. Nguyen, L. Ungur, *Chem. Eur. J.* **2022**, *28*, e202200227.
[107] F. Liu, G. Velkos, D. S. Krylov, L. Spree, M. Zalibera, R. Ray, N. A. Samoylova, C.-H. Chen, M. Rosenkranz, S. Schiemenz, F. Ziegs, K. Nenkov, A. Kostanyan, T. Greber, A. U. B. Wolter, M. Richter, B. Büchner, S. M. Avdoshenko, A. A. Popov, *Nat. Commun.* **2019**, *10*, 571.
[108] F. Liu, D. S. Krylov, L. Spree, S. M. Avdoshenko, N. A. Samoylova, M. Rosenkranz, A. Kostanyan, T. Greber, A. U. B. Wolter, B. Büchner, A. A. Popov, *Nat. Commun.* **2017**, *8*, 16098.
[109] Y. Wang, J. Xiong, J. Su, Z. Hu, F. Ma, R. Sun, X. Tan, H.-L. Sun, B.-W. Wang, Z. Shi, S. Gao, *Nanoscale* **2020**, *12*, 11130–11135.
[110] Y. Wang, G. Velkos, N. J. Israel, M. Rosenkranz, B. Büchner, F. Liu, A. A. Popov, *J. Am. Chem. Soc.* **2021**, *143*, 18139–18149.
[111] C. Zener, *Phys. Rev.* **1951**, *82*, 403–405.
[112] C. Coulon, H. Miyasaka, R. Clérac, *Single-Molecule Magnets and Related Phenomena* (Ed.: R. Winpenny), Springer Berlin Heidelberg, Berlin **2006**, pp. 163–206.
[113] C. Coulon, R. Clérac, L. Lecren, W. Wernsdorfer, H. Miyasaka, *Phys. Rev. B* **2004**, *69*, 132408.
[114] L. Lecren, O. Roubeau, C. Coulon, Y.-G. Li, X. F. Le Goff, W. Wernsdorfer, H. Miyasaka, R. Clérac, *J. Am. Chem. Soc.* **2005**, *127*, 17353–17363.
[115] A. Bencini, D. Gatteschi, Electron Paramagnetic Resonance of Exchange Coupled Systems, Springer Berlin Heidelberg, Berlin **1990**, pp. 86–120.
[116] V. Vieru, N. Iwahara, L. Ungur, L. F. Chibotaru, *Sci. Rep.* **2016**, *6*, 24046.
[117] R. Boča, *Coord. Chem. Rev.* **2004**, *248*, 757–815.
[118] S. Ferlay, T. Mallah, R. Ouahès, P. Veillet, M. Verdaguer, *Nature* **1995**, *378*, 701–703.
[119] F. Donati, A. J. Heinrich, *Appl. Phys. Lett.* **2021**, *119*, 160503.
[120] A. Singha, P. Willke, T. Bilgeri, X. Zhang, H. Brune, F. Donati, A. J. Heinrich, T. Choi, *Nat. Commun.* **2021**, *12*, 4179.
[121] G. Gabarró-Riera, G. Aromí, E. C. Sañudo, *Coord. Chem. Rev.* **2023**, *475*, 214858.

[122] F. Allouche, G. Lapadula, G. Siddiqi, W. W. Lukens, O. Maury, B. Le Guennic, F. Pointillart, J. Dreiser, V. Mougel, O. Cador, C. Copéret, *ACS Cent. Sci.* **2017**, *3*, 244–249.
[123] M. D. Korzyński, Z. J. Berkson, B. Le Guennic, O. Cador, C. Copéret, *J. Am. Chem. Soc.* **2021**, *143*, 5438–5444.
[124] F. Donati, S. Rusponi, S. Stepanow, L. Persichetti, A. Singha, D. M. Juraschek, C. Wäckerlin, R. Baltic, M. Pivetta, K. Diller, C. Nistor, J. Dreiser, K. Kummer, E. Velez-Fort, N. A. Spaldin, H. Brune, P. Gambardella, *Phys. Rev. Lett.* **2020**, *124*, 077204.
[125] F. Donati, S. Rusponi, S. Stepanow, C. Wäckerlin, A. Singha, L. Persichetti, R. Baltic, K. Diller, F. Patthey, E. Fernandes, J. Dreiser, Ž. Šljivančanin, K. Kummer, C. Nistor, P. Gambardella, H. Brune, *Science* **2016**, *352*, 318–321.
[126] F. D. Natterer, F. Donati, F. Patthey, H. Brune, *Phys. Rev. Lett.* **2018**, *121*, 027201.
[127] O. Kahn, J. Larionova, L. Ouahab, *Chem. Commun.* **1999**, 945–952.
[128] L. Catala, T. Mallah, *Coord. Chem. Rev.* **2017**, *346*, 32–61.
[129] Y.-w. Jun, J.-w. Seo, J. Cheon, *Acc. Chem. Res.* **2008**, *41*, 179–189.

Manuscript received: March 2, 2023
Accepted manuscript online: August 4, 2023
Version of record online: September 29, 2023